Response to comments of Reviewer 1

Authors would like to express sincere thanks to an anonymous reviewer for his/her valuable comments. We revised a manuscript very carefully based on given comments. The comments of the reviewer are in blue, our replies are in black, and changes made in the revised manuscript are in red. Our replies to the comments are as below.

The article entitled Retrieval of cloud properties from sky radiometer observed spectral zenith radiances, by P. Khatri, H. Iwabuchi, T. Hayasaka, H. Irie, T. Takamura, A. Yamazaki, A. Damiani, H. Letu and Q. Kai presents and validates a method for retrieving cloud properties (i.e. cloud optical depth and Cloud effective radius) from zenith radiance measurements of the sky, performed from ground with a commercial available sun-sky radiometer Prede POM02.

The article is considered important and presents a method that means a step forward in the establishment and improvement of ground based methods for the observation of cloud properties, that are one of the most important factors in the Earth climate. The establishment, validation, and further improvement of the method will allow other users of the Prede POM02 sun-sky radiometer, particularly users of the SKYNET international network, to obtain relevant information and contribute to this field of research. The study is considered adequate for this journal. However, the article would benefit of a final revision by a native English speaker.

➔ Thank you for your encouraging comments. The revised manuscript has been read by a native English speaker.

Specific comments:

- Abstract, line 17: the procedure of deriving calibration constants from another instrument could be called "calibration transfer method".

➔ It is done in the revised manuscript (**Line 17**).

- Line 34-35: please rewrite sentence ("unlike advancements"?)

➔ Those sentences are rewritten as below (**Line 32 – Line 35**).

Compared with the routine observation of aerosols through surface networks, such as AERONET (https://aeronet.gsfc.nasa.gov/) and SKYNET (http://atmos3.cr.chiba-u.jp/skynet/), observation of clouds from the surface is performed at a limited number of stations and most of the observation data are not easily accessible.

- Line 47: not sure "tally" is the most appropriate word here

➔ We rewrote the sentence as below (**Line 44 – Line 46**).

The fundamental idea is to compare the observed signals with LUT data corresponding to prior known cloud optical depth (COD) and cloud particle effective radius (CER) while finding a plausible solution for the COD and CER combination.

- Line 80: you have included 940 nm channel in the list of channels used for aerosol retrieval?

➔ It is corrected in the revised manuscript (**Line 75 – Line 76**).

- Line 89 and 91: instead of "alternation", "alternative" could suit best

➔ It is done in the revised manuscript (**Line 84 & Line 85)**.

- Line 92: rewrite "A more detailed study about..."

➔The typo mistake has been corrected. In the revised manuscript, the sentence appears as (**Line 86 - Line 87)**.

A more detailed study about sky radiometers and their calibrations can be found in Khatri et al. (2016).

- Line 96-98: authors state that 2.2um channel is not used because the longest wavelength used by AERONET is 1.627um, but Cimels are not used in this study. Do the authors plan to apply the method on Cimel instruments in the future? Otherwise, I think it is not well understood the reason for rejecting this channel.

➔We clarified the reasons in the revised manuscript as below (**Line 90 - Line 95)**.

We use sky radiances (E) observed at three longer wavelengths (0.87, 1.02, and 1.627 μm), excluding 2.2 μm, which is not used for two main reasons. First, our statistical analysis suggests that the number of unphysical data (observation data recorded as 0) for 2.2 μm is high; thus, 2.2 μm is excluded to increase the retrieval number. Second, the longest wavelength used by AERONET is 1.64 μm; so the proposed algorithm could be easily used for sun photometer observed data as well. Wavelengths shorter than 0.87 μm are not used to avoid the effect of aerosols as far as possible.

- Line 103: "from the solar disk scan during very clear sky days"

➔ The sentence is corrected as suggested by the reviewer as (**Line 99 - Line 100)**

$\Delta\Omega$ for 0.87, 1.02, and 1.627 μm can be determined from the solar disk scan during very clear sky days (Nakajima et al., 1996)

- Line 105: "wavelengths"

➔ The typo mistake is corrected in the revised manuscript (**Line 101)**.

- Line 111: "very mere" -> very small

➔ A correction is made as suggested by the reviewer in the revised manuscript (**Line 106)**.

–Line 113: do the authors expect any limitation in the method for cases of dust mixed with clouds due to non-sphericity?

➔We used aerosol data of very clear sky days while determining the calibration constant (F_0) values using the proposed method. Thus, there is a very little chance of mixing clouds with aerosols as suggested by the reviewer. However, even if some cloudy data have been misinterpreted as aerosols by a cloud-screening procedure, such cloudy data can get filtered because the proposed method eliminates the outlier that decreases the correlation coefficient between lnF and τm (F, τ, and m are measured direct intensity, total optical thickness and optical air mass, respectively) through an iteration process until a very strong correlation (r ≥ 0.997) is obtained (**Line 113 – Line 115)**.

–Line 116: Beer-Lambert

➔ The typo mistake is corrected in the revised manuscript (**Line 112)**.

- Line 120: do the authors use any minimum number of data points to perform a successful final IL fit? Any other threshold or criteria?

➔ There is no specific condition regarding minimum number of data points because each final IL plot is visually inspected to confirm that suspicious data points are not included and there are enough number of data points in the fit.

The proposed method was designed by putting other criteria, such as the maximum value of aerosol optical thickness (AOT) and solar zenith angle, as well. However, our test indicates that such criteria can have a very less influence in overall performance because the outlier is removed through iteration as explained in the reply of the previous comment. Thus, criteria other than the value of correlation coefficient are removed (**Line 113 – Line 115)**.

- Line 129: "temporal variation of lnF0"

➔ The sentence is corrected as below (**Line 123 – Line 124)**.

Thus, the proposed method can be used to determine temporal variation of $lnF_{0,1.627}$, which is useful for analyzing long-term observation data by mitigating the filter degradation problem.

- Line 154-155: "calculated for COD and CER in the intervals 1-64 and 2-32 respectively, with steps of 1"

➔The sentence is corrected as below (**Line 158 – Line 159)**.

The retrieval errors are calculated for COD and CER values in the ranges of 1–64 and 2–32 µm, respectively, in steps of 1 µm.

- Line 160: the assumed error of 1.0 cm for PWC looks like a very high upper estimation of error. Is it a typo error?

➔ There was no typo mistake for assumed error of PWC; however, there was a typo mistake for assumed value of PWC. The assumed value of PWC was 1.5 cm (it was mistakenly written as 1.0 cm). It is corrected in the revised manuscript. We assumed error value of this magnitude to better understand the algorithm performance (**Line 164**).

- Lines 169-203: it is a long paragraph. Perhaps it could be divided at lines 183 and 191

➔ It is done in the revised manuscript (**Line 186 & Line 193**).

- Lines 213-214: do the three percentages correspond respectively to percentiles 5, 50 and 95?

➔ Yes, they are according to the reviewer. The English writing of the revised manuscript has been polished by a native speaker. Thus, each sentence is expected to have a clear meaning in the revised manuscript (**Line 214 – Line 216**).

- Line 217: comparison, not compassion

➔ This typo mistake is corrected in the revised manuscript (**Line 218**).

- Line 221 (section 5.1). Is the NA radiometer a pirheliometer? Is it pointing at nadir direction continuously? Does it really measure radiance, or irradiance? I think it would useful to have some more details about the instrumentation used here.

➔ The description is elaborated in the revised manuscript as below (**Line 223 - 229**).

The broad-band radiance and irradiance of the shortwave spectral range (0.3 – 2.8 μm) observed using a narrow-angle radiometer (EKO Instruments Co., Ltd., Japan; FOV: 5°) and a pyranometer (Kipp and Zonen, Netherlands; FOV: 180°), respectively, at Chiba (35.62°N, 140.10°E) every 20 s from December 2015 to December 2016 are used to evaluate the cloud properties observed by the sky radiometer. The narrow-angle radiometer observes the downwelling irradiance signals as voltage in a narrow FOV. The instrument was calibrated by the manufacturer in the laboratory, and the observed signals are converted into radiance (unit: $W/m^2/sr$) by using the company provided calibration constant value. Because the narrow-angle radiometer faces upward, thus obtained radiance is from the zenith.

- Line 236: "highly qualitative"?

➔ "qualitative enough" is used instead of "highly qualitative" in the revised manuscript (**Line 240**).

- Section 5.2.: in order to better understand the improvement of the comparison respect to Kathri 2018, a short mention to the previous results using all the database would be useful

➔As suggested by the reviewer, a new paragraph is added in section 5.2 (**Line 283 – Line 289**).

Although the qualitive information reported by Khatri et al. (2018) and the comparisons in Figures 7 and 8 of this study are similar, there are differences in Figures 7 and 8 with the comparison plots shown in Khatri et al. (2018). The application of data screening criteria in this study generally screened out data with large differences between the sky radiometer and satellite sensors. These large differences in the previous comparison probably arose from the different FOVs of the satellite sensor and sky radiometer, while observing inhomogeneous clouds. Thus, the comparison results presented in this study by addressing the cloud inhomogeneity problem more logically should give more accurate and refined information than those presented in Khatri et al. (2018).

Figures: - Line 270: Figures 7a and 7b

➔ The typo mistake is corrected in the revised manuscript (**Line 272**).

- Line 276: Figures 8a and 8b

➔ The typo mistake is corrected in the revised manuscript (**Line 277**).

- Figure 4: I understand that figures a, b, c correspond to channels 870, 1020 and 1627. But I do not understand what are zenith and azimuth angles respectively. If both zenith and azimuth results are the same for figures a and b, but are slightly different for figure c, please state that zenith and azimuth angles are represented with different colors.

➔The zenith and azimuth angles are exactly same for Figs. 4a, 4b, and 4c. Since the transmittance changes with the solar position, we choose solar zenith and azimuth angles of 30° and 0° as representative to investigate how the transmittances of 0.87, 1.02, and 1.627 μm change with the changes of COD and CER. Therefore, the solar zenith and azimuth angles are indicated in the caption.

If Fig. 4c is viewed very carefully, the contour lines denoted by different colors for 2 < COD < 5 and CER > 4 μm appear again for ~2 < COD < 4 and CER < 4 μm. It is technically difficult (due to not sufficient space) to write the values of transmittances within the contour lines (similar to Figs. 4a and 4b) in the second domain, i.e., ~2 < COD < 4 and CER < 4 μm. Therefore, different colors are used to resolve this technical difficulty (**Line 443 - 446**).

References

Nakajima, T., Tonna, G., Rao, R., Kaufman, Y., and Holben, B. N. : Use of sky brightness measurements from ground for remote sensing of particulate polydispersions, Appl. Opt., 35(15), 2672–2686, https://doi.org/10.1364/AO.35.002672, 1996.

Khatri, P., Takamura, T., Estellés, V., Irie, H., Kuze, H., Campanelli, M., Sinyuk, A., Lee, S.-M., Sohn, B. J., Pandithurai, G., Kim, S.-W., Yoon, S. C., Martinez-Lozano, J. A., Hashimoto, M., Devara, P. C. S., and Manago, N.: Factors for inconsistent aerosol single scattering albedo between SKYNET and AERONET, J. Geophys. Res., 121(4), 1859-1877, https:/doi.org/10.1002/20159JD023976, 2016.

Khatri, P., Hayasaka, T., Iwabuchi, H., Takamura, T., Irie, H., and Nakajima, T. Y.: Validation of MODIS and AHI observed water cloud properties using surface radiation data, J. Meteor. Soc. Japan, 96B, 151-172, https:/doi.org/10.2151/jmsj.2018-036, 2018.

Response to comments of Reviewer 2

Authors would like to express sincere thanks to an anonymous reviewer for his/her valuable comments. We revised a manuscript very carefully based on given comments. The comments of the reviewer are in blue, our replies are in black, and changes made in the revised manuscript are in red. Our replies to the comments are as below.

The development of the algorithm in this study is important because it is of great merit for radiometers to make their self-calibrations on-site. However, there are some issues to be clarified before publication finally, in terms of the detailed points below. In addition, it is recommended to have the manuscript English-proofed.

➔ Thank you for your encouraging comment. The manuscript has been read by a professional native English speaker.

Specific comments:

L67-68 "We use three carefully selected wavelengths to retrieve COD and CER simultaneously." How did the authors carefully select the wavelengths?

➔ They are described in the revised manuscript as below (**Line 90 – Line 95**).

We use sky radiances (*E*) observed at three longer wavelengths (0.87, 1.02, and 1.627 μm), excluding 2.2 μm, which is not used for two main reasons. First, our statistical analysis suggests that the number of unphysical data (observation data recorded as 0) for 2.2 μm is high; thus, 2.2 μm is excluded to increase the retrieval number. Second, the longest wavelength used by AERONET is 1.64 μm; so the proposed algorithm could be easily used for sun photometer observed data as well. Wavelengths shorter than 0.87 μm are not used to avoid the effect of aerosols as far as possible.

L95 Fig. 1 Do the authors specify some criterion for the number of iteration? Do all the observed data properly retrieved?

➔ The total number of iterations is set as 50. If the solution does not converge within 50 iterations, the analysis is discarded (**Line 144 – Line 145**).

L181 Fig.4 From Fig.4, it seems that transmittances of the three wavelengths have dual values for a certain effective radius of cloud droplet. For example, the values 0.7 of transmittance appear at two regions of cloud optical depth more than and less than 10. The situation might cause the problem of dependency on a-priori or a starting value of the iteration in Fig. 1 and x_a in Eq. 2. Does the issue is not critical for this study?

➔The *a-priori* values are climatological data sets, and they are fixed in the algorithm. The starting values of COD and CER can have an important effect in the retrieval as suggested by the reviewer. Our approach to overcome this problem is described in the revised manuscript as below (**Line 145 – Line 154**).

As highlighted in Sections 1 and 4, transmittance signals may not always be characterized by unique COD or CER values. Consequently, the initial values of COD and CER used for iteration can be important when searching the plausible set of COD and CER values. To address this important issue, we first approximate the initial COD and CER values to start the iteration. The approximation is done by searching a set of COD and CER values by comparing observed $T_{1.627}/T_{1.02}$ and $T_{1.02}$ with LUT of corresponding values modeled for COD values of 1–64 and CER values of 2–32 μm in steps of 1 μm. $T_{1.627}/T_{1.02}$ generally decreases with the increase of COD; whereas when COD increases, $T_{1.02}$ increases first until reaching the peak value, and then starts to decrease. Thus, $T_{1.627}/T_{1.02}$ and $T_{1.02}$ can be used simultaneously to determine the range of COD and CER in which the true values are likely to fall. A set of COD and CER values that generate the smallest root mean square difference between the observed and modeled values is used for the initial values in the iteration.

L199 "Note that the absorption tends to reduce T( ), whereas the forward scattering tends to increase it." In terms of cloud retrieval, multiple scattering is important for larger COD, which will enhance the forward scattering and absorption processes.

➔We refined the sentences as suggested by the reviewer as (**Line 199 – Line 201**)

Both the forward scattering and absorption can increase with the increase of COD along with the increase in multiple scattering; the increase in $T(\lambda)$ before the peak value is due to the dominance of forward scattering over absorption, and vice versa for the decrease in $T(\lambda)$ after the peak value.

L223-224 "a narrow-angle (NA) radiometer (FOV: 5)" The observation was conducted in the zenith direction same as the sky radiometer?

➔ We provided information below to clarify this issue (**Line 227 – Line 229**).

The instrument was calibrated by the manufacturer in the laboratory, and the observed signals are converted into radiance (unit: W/m^2/sr) by using the company provided calibration constant value. Because the narrow-angle radiometer faces upward, thus obtained radiance is from the zenith.

Fig. 6 The slope of the solid line should be multiplied by 2*phi. Currently, the pyranometer observation seems overestimated greatly, compared with narrow angle radiometer, which might mislead to inconsistency of the two observations.

➔As suggested by the reviewer, the slope of the solid line is multiplied by 2*phi (**Page 18**).

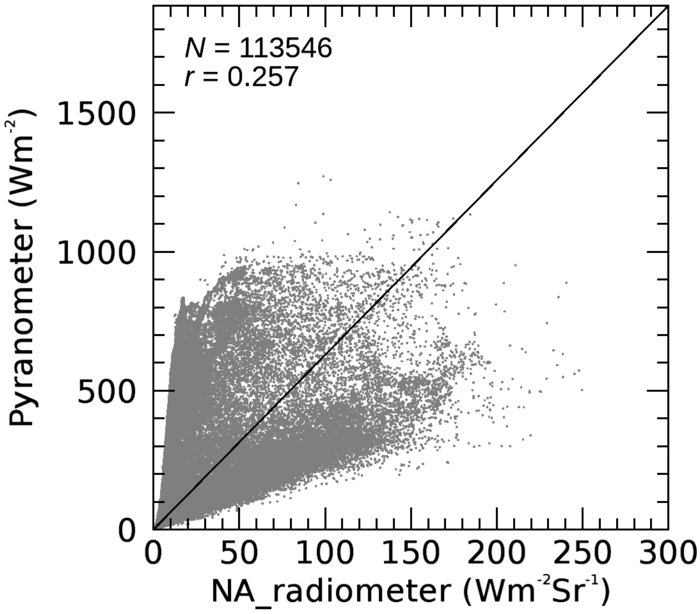

Figure 6: Scatterplot of broad-band radiances and irradiances observed with a narrow-angle radiometer and a wide-angle pyranometer at Chiba (35.62°N, 140.10°E) during January–March 2016. The solid line represents $y = 2\pi x$.

The solid line hardly suggests the overestimation from pyranometer as data points are scattered in both sides of a solid line. On the other hand, it indicates the asymmetric distribution of radiance.

Technical corrections:

L28 "Foster" -> "Forster"

➔ It is corrected in the revised manuscript (**Line 28**).

L59 "MCBride" -> "McBride"

➔ It is corrected in the revised manuscript (**Line 56**).

L120 "(r)" rather than "(r^2)"

➔ It is done in the revised manuscript (**Line 115**).

L163 "priory" -> "a priori"

➔ It is corrected in the revised manuscript (**Line 167**).

L169 Fig. 3b, 3e, 3h, and 3k The style of right axis should be same as the other panels.

➔ They are done in the revised manuscript (**Page 15**).

L236 "qualitative" -> "quantitative" ?!

➔ It is qualitative (**Line 240**).

L270 "Figures 6(a) and 6(b)" -> "Figures 7a and 7b"

➔They are corrected in the revised manuscript (**Line 272**).

Figure 7, Legends: Please omit the dual markers for each site.

➔They are done in the revised manuscript (**Page 18 & page 19**).

L276 "Figs. 7(a) and 7(b)" -> "Figs. 8a and 8b"

➔They are corrected in the revised manuscript (**Line 277**).

Changes made by authors to address the reviewers' comments

Formatted: Font: 24 pt

Formatted: Centered

Retrieval of cloud properties from sky radiometer observed spectral zenith radiances

Pradeep Khatri[1], Hironobu Iwabuchi[1], Tadahiro Hayasaka[1], Hitoshi Irie[2], Tamio Takamura[2], Akihiro Yamazaki[3], Alessandro Damiani[2], Husi Letu[4], Qin Kai[5]

[1]Center for Atmospheric and Oceanic Studies, Graduate School of Science, Tohoku University, Sendai, Japan

[2]Center for Environmental Remote Sensing, Chiba University, Chiba, Japan

[3]Meteorlogical Research Institute, Tsukuba, Japan

[4]Institute of Remote Sensing and Digital Earth, Chinese Academy of Sciences, Beijing, China

[5]School of Environment and Geoinformatics, China University of Mining and Technology, Xuzhou, China

Correspondence to: Pradeep Khatri (pradeep.khatri.a3@tohoku.ac.jp)

Abstract: An optimal-estimation based algorithm to retrieve cloud optical thickness (COD) and cloud-particle effective radius (CER) from spectral zenith radiances observed by a narrow field of view (FOV) ground-based sky radiometer is developed. To further address the filter-degradation problem while analyzing data of long-term observation, an on-site calibration procedure is proposed, which is found to have a very good accuracy with respect to a standard procedure, i.e., a calibration transfer method. An error evaluation study conducted by assuming errors in observation-based transmittances and ancillary data of water vapor concentration and surface albedo suggests that the errors in input data can influence retrieved CER more effectively than COD. Except for some narrow domains that fall within COD < 15, the retrieval errors are very small for both COD and CER. The retrieved cloud properties are found to reproduce the broadband radiances observed by a narrow FOV radiometer more precisely than broadband irradiances observed by a wide FOV pyranometer, justifying the quality of retrieved product (at least COD) and, at the same time, indicating the important influence of instrument FOV in cloud remote sensing. Further, CODs (CERs) between sky radiometer and satellite observations show fairly good (poor) agreement.

Deleted:

Deleted: procedure of deriving calibration constants using a master instrument

1 Introduction

Clouds play an important role to drive the climate system and hydrological cycle (Rosenfeld et al., 2014). Their accurate representation in the global climate model remains one of the largest uncertainties (Forster et al., 2007). Clouds are being observed from the space by using various sensors onboard various satellites, which are greatly helping the scientific community to understand more about cloud characteristics and their roles on climate system, hydrological cycle, and so on. Despite such profound scientific implication, the quality assurance of such satellite observed cloud properties has always become an important task in the field of cloud remote sensing. It has been recognized as a challenging task primarily due to the lack of enough standard data representing different atmospheric conditions to perform quality assessment. In comparison to routine observation of aerosols through surface networks such as AERONET (https://aeronet.gsfc.nasa.gov/) and SKYNET (http://atmos3.cr.chiba-u.jp/skynet/), clouds are being observed routinely from the surface at a very limited stations, and most of those observation data are not easily accessible. Taking into account of multiple stations of above-mentioned ground-based networks around the world, cloud observations from them should be strengthen as their operating instruments for aerosol observation are capable for cloud observation as well. This can greatly help satellite remote sensing community to validate the cloud products and the whole cloud research community to study clouds in more detail by using high resolution surface data. This recognition strongly motivated this study.

It is important to mention that efforts have been made in the past for studying clouds from the surface by using zenith radiances observed by radiometers belonging to AERONET (e.g., Chiu et al., 2010, 2012) and SKYNET (e.g., Kikuchi et al., 2006). In accordance with the literature, the radiometers belonging to AERONET and SKYNET are termed as sun photometer and sky radiometer, respectively from here. Similar to space-based cloud remote sensing using reflected signals (e.g., Nakajima and King, 1990), those studies using data of sun photometer and/or sky radiometer are based on a framework of a look-up-table (LUT) use. The fundamental idea is to compare observed signals with data of LUT corresponding to priory known cloud optical depth (COD) and cloud-particle effective radius (CER) while finding the plausible solution for COD and CER combination. This signal can be zenith radiance or transmittance. Chiu et al. (2010) retrieved COD from LUT of zenith radiances of water non-absorbing wavelengths constructed by assuming a fixed CER; Chiu et al. (2012) and Kikuchi et al. (2006) used LUT of transmittances of water non-absorbing and absorbing wavelengths to infer COD and CER simultaneously. It is important to note that the reflected signals for water non-absorbing and absorbing wavelengths can have nearly one-to-one relationships with COD and CER, respectively. On the other hand, such behaviors cannot be seen for transmitted signals, making the retrieval process very difficult for LUT based approach using transmitted signals. In addition, unlike reflected signal, the transmitted signal is weakly sensitive to CER change. This again adds complexity in the retrieval while using transmitted signals. Further, the shape of LUT is subject to change depending on the change of solar position, making the retrieval process more cumbersome, if LUTs developed for a limited number of specific solar positions are used. To overcome such difficulties, some innovative techniques have been proposed in the past. For example, McBride et al. (2011) developed a spectral method by using the slope of the transmittances of 13 wavelengths in between 1565nm and 1634nm and transmittance at the visible wavelength of 515nm to retrieve COD and CER simultaneously. LeBlanc et al. (2015) derived 15 parameters to quantify spectral variations in shortwave transmittances due to absorption and scattering of liquid water and ice clouds, manifested by shifts in spectral slopes, curvatures, maxima, and minima to discriminate cloud phase and retrieving COD and CER. Unfortunately, those techniques developed for radiometers of high spectral resolution are less suitable for both sun photometer and sky radiometer because they have a very limited number of channels.

Taking above-mentioned difficulties in mind, we develop a retrieval algorithm based on optimal-estimation method, i.e., a maximum a posteriori (MAP) method (Rodgers, 2000). We use three carefully selected wavelengths to

Deleted: Unlike advancement in aerosol observation

Deleted: tally

Deleted: of signals

Deleted: MCBride

retrieve COD and CER simultaneously. Further, an on-site calibration method is proposed to cope the filter degradation problem while analyzing data of long-term observation. Though the algorithm is developed by using data of sky radiometer, it is equally applicable for data of sun photometer.

This study is designed in the following way: A brief description of sky radiometer is given in section 2. The methodology, retrieval error, and quality assessment of retrieved products are discussed in sections 3, 4 and 5, respectively. Finally, the conclusion is presented in section 6.

2 Sky radiometer

The sky radiometer (Model: POM-02), manufactured by PREDE Co. Ltd., Japan, is an instrument capable to make observations of direct intensity, angular sky radiance (both almucantar and principle plane scans), and zenith sky radiance at 11 wavelengths at specified time interval. The field of view (FOV) is 1°. The most commonly used wavelengths by SKYNET are 0.315, 0.34, 0.38, 0.4, 0.5, 0.675, 0.87, 0.94, 1.02, 1.627, and 2.2 µm. Among them, the direct and angular sky radiances at the wavelengths of 0.34, 0.38, 0.4, 0.5, 0.675, 0.87, and 1.02 µm, at which the absorptions by atmospheric gases and water/ice are negligible, are in use for aerosol remote sensing (Nakajima et al., 1996; Hashimoto et al., 2012); the direct intensities observed at the wavelengths of 0.315 µm and 0.94 µm are in use for remote sensing of ozone (Khatri et al., 2014) and water vapor (e.g., Campanelli et al., 2014), respectively. The zenith sky radiances have different potential applications from different perspectives. Currently, the zenith sky radiances of cloudy skies have been used for cloud remote sensing (e.g., Kikuchi et al., 2006). The calibration constant terms for sky radiance (both angular and zenith) and direct intensity are required while deriving physical data from observation signals via retrieval algorithms. One of the largest benefits of PREDE sky radiometer is that those calibration constants can be obtained from field observation data themselves as outlined by Nakajima et al. (1996). In brief, an Improved Langley (IL) method (Nakajima et al., 1996; Campanelli et al., 2004), which is an alternative of Normal Langley (NL) method, can be used to obtain calibration constants for direct intensities. Similarly, the solar disk scan method, which can be alternative of integrating sphere based method, can be used to determine the calibration constant for sky radiances. A more detailed study about sky radiometer and its calibration can be found in Khatri et al. (2016).

3 Methodology

The schematic diagram of the study method is shown in Fig. 1. We use sky radiances (E) observed at three longer wavelengths (0.87, 1.02, and 1.627 µm) excluding 2.2 µm. The longest wavelength of 2.2 µm is not used mainly for two important reasons: First, our statistical analysis suggests that the number of unphysical data (observation data recorded as 0) for 2.2 µm is high; thus, 2.2 µm is excluded to increase the retrieval number. Second, taking into account the longest wavelength adopted by AERONET as 1.64 µm, the proposed algorithm has a potential application for sun photometer observed data as well. The wavelengths shorter than 0.87 µm are not used to avoid the effect of aerosols as far as possible. The observed E can be converted to the transmittance (T) by the equation below:

Deleted: 0.94,

Deleted: alternation

Deleted: alternation

Deleted: using

Deleted: etc.,

Deleted:

Deleted: considering the application of proposed algorithm for sun photometer data as well because the longest wavelength used by AERONET is 1.64 µm.

Deleted: Similarly, the shorter

$$T(\lambda) = \frac{\pi E(\lambda)}{\mu_0 \Delta\Omega(\lambda) F_0(\lambda)}, \qquad (1)$$

where μ_0 is the cosine of the solar zenith angle, $\Delta\Omega$ is the calibration constant for sky radiance, which is also termed as solid view angle in SKYNET community, F_0 is the calibration constant for direct intensity, and λ is the wavelength. $\Delta\Omega$ for those three wavelengths can be determined from the solar disk scan during very clear sky days (Nakajima et al., 1996). Though the current IL method can be used to determine temporal F_0 for the first two wavelengths (0.87 and 1.02 µm), it is less applicable for water absorbing wavelengths, such as 1.627 µm. For 1.627 µm, one may use F_0 derived from NL method, but NL is less practical to be conducted routinely within short time interval (e.g., each month) to derive temporal F_0. We prefer to use temporal F_0 for all wavelengths to take into account of filter degradation with time (e.g., Khatri et al., 2014). To derive temporal F_0 at 1.627 µm, we use an alternative method of IL as proposed by Khatri et al. (2014). In brief, aerosol data (refractive index and volume size distribution) and direct intensity observed at 1.627 µm ($F_{1.627}$) are used. Note that aerosol optical thickness (τ_{aer}) depends primarily on aerosol size distribution, and the refractive index has a very small contribution to τ_{aer} (King, 1978; Khatri and Ishizaka, 2007). Thus, the refractive index at the wavelength of 1.02 µm, which is the highest wavelength for routine aerosol retrieval, is assumed to be same for 1.627 µm while calculating τ_{aer} at 1.627 µm from volume size distribution using Mie calculation. The optical air mass (m) and sun-earth distance (R) are calculated from latitude and longitude of observation site and observation time. Similarly, the Rayleigh-scattering optical depth at 1.627 µm ($\tau_{Ray,1.627}$), though very small in magnitude, is calculated from the atmospheric pressure of observation site. Finally, the Beer-lambert law of $ln(F_{1.627}R^2) = lnF_{0,1.627} - (\tau_{aer} + \tau_{Rayleigh})m$ is used to determine $lnF_{0,1.627}$, i.e., the natural logarithm of the calibration constant of direct intensity at 1.627 µm. It is done by using data of all clear sky periods of each month by correlating $ln(F_{1.627}R^2)$ with $(\tau_{aer} + \tau_{Rayleigh})m$. The outlier that deteriorates the correlation utmost is detected and removed in each iteration till the condition of correlation coefficient ($r \geq 0.997$) is satisfied. To understand the quality of thus calculated $lnF_{0,1.627}$ values, we compare them with data determined from independent standard method. The standard method refers to the method of deriving calibration constant by performing collocated observation of a field and master instruments together. In Fig. 2, the comparison is shown for three different sky radiometers operated at the observation sites of Hedo-misaki (26.87°N, 128.25°E), Fukue-jima (32.75°N, 128.68°E), and Sendai(38.26°N,140.84°E). Figure 2 shows a very good agreement between our method and the standard method for all three sky radiometers. Figure 2 also shows a relative difference. The relative difference (in percentage) is defined as the difference between our method and the standard method normalized by the value of the standard method. The relative difference can be seen to be less than 0.05% for all sky radiometers. This confirms the soundness of proposed method, which is not only inexpensive, but also very easy. Thus, the proposed method can be used to determine temporal variation of $lnF_{0,1.627}$, which is very useful while analyzing data of long-term observation by coping filter degradation problem. By using volume size distribution and refractive indices of respective wavelengths, the proposed method can be used for first two wavelengths as well. There is negligible difference in the values obtained between IL method and this method for the first two wavelengths. This study uses the

Deleted: of

Deleted: mere

Deleted: beer

Deleted: ^{2})

Deleted: 995

values obtained from the proposed method for all wavelengths to avoid the difficulty of reading lnF_0 from different files.

Along with T values of three wavelengths obtained from Eq. (1), we use precipitable water content (PWC) and spectral surface albedo data. They are obtained from radiosonde observation (http://weather.uwyo.edu/upperair/sounding.html) and MODIS observation (product name: MCD43A4), respectively. Finally, COD and CER are retrieved simultaneously by minimizing the cost function (J) below:

$$J = (\boldsymbol{x} - \boldsymbol{x}_a)^T \boldsymbol{S}_a^{-1} (\boldsymbol{x} - \boldsymbol{x}_a) + [\boldsymbol{y} - \boldsymbol{F}(\boldsymbol{x}, \boldsymbol{b})]^T \boldsymbol{S}_y^{-1} (\boldsymbol{y} - \boldsymbol{F}(\boldsymbol{x}, \boldsymbol{b})] \quad , \tag{2}$$

where $\boldsymbol{x}$ is a state vector, $\boldsymbol{x_a}$ is an a priori vector, $\boldsymbol{S_a}$ and $\boldsymbol{S_y}$ are error covariance matrices for the a priori and measurement, respectively, $\boldsymbol{y}$ is the measurement vector, $\boldsymbol{F}$ is the forward model, and $\boldsymbol{b}$ is the model parameter vector (ancillary data) . The terms $\boldsymbol{x}$, $\boldsymbol{y}$, and $\boldsymbol{b}$ are defined as:

$$\boldsymbol{x} = \begin{pmatrix} ln\tau \\ lnr_e \end{pmatrix}, \ \boldsymbol{y} = \begin{pmatrix} lnT_{1.627} \\ lnT_{1.02} \\ lnT_{0.87} \end{pmatrix}, \text{ and } \boldsymbol{b} = \begin{pmatrix} W \\ A_{1.627} \\ A_{1.02} \\ A_{0.87} \end{pmatrix},$$

where τ and r_e represent COD and CER, respectively; W and A_λ represent PWC and surface albedo at wavelength λ, respectively. Both $\boldsymbol{S_a}$ and $\boldsymbol{S_y}$ are assumed to be diagonal matrices. $\boldsymbol{x_a}$ and the diagonal elements of $\boldsymbol{S_a}$ are determined from one-year data of water cloud properties observed over Japanese SKYNET sites by Advanced Himawari Imager (AHI) sensor onboard Himawari-8, a Japanese geostationary satellite. The diagonal terms for $\boldsymbol{S_y}$ are determined based on simulation of perturbations in $T(\lambda)$ generated from 300 random gaussian noises of error sources discussed in section 4. The Santa Barbara DISORT Atmospheric Radiative Transfer (SBDART) model (Ricchiazzi et al., 1998) is used for forward modelling, and the Levenberg-Marquardt method is used to minimize the cost-function. The total number of iteration is set to 50. If the solution does not converge within 50 iterations, the analysis is discarded. As highlighted in section 1 and shown in section 4, transmittance signals may not always be characterized by a unique COD and/or CER. As a result, initial values of COD and CER used for iteration can keep a great importance while searching the plausible set of COD and CER. To address this important issue, we first approximate the initial values of COD and CER to start the iteration. It is done by searching a set of COD and CER through a comparison of observed $T_{1.02}/T_{1.627}$ and $T_{1.02}$ with LUT of corresponding values modeled for COD ranging from 1 – 64 and CER ranging from 2 – 32 µm at step of 1. $T_{1.02}/T_{1.627}$ decreases with the increase of COD; whereas when COD increases, $T_{1.02}$ increases first until reaching the peak value, and then starts to decrease. Thus, simultaneous use of $T_{1.02}/T_{1.627}$ and $T_{1.02}$ can help one to figure out the range of COD and CER, in which the true values are likely to fall. A set of COD and CER that can generate a least root mean square difference between observed and modeled values is used as initial values in the iteration.

4 Retrieval error

In order to understand the performance of the proposed algorithm for different types of input data (transmittance and ancillary data), retrieval errors are calculated by assuming errors on them. The retrieval errors are calculated for COD and CER in the intervals of 1 - 64 and 2 - 32 µm respectively, with steps of 1. The simulations are performed for

Formatted: Font: 10 pt

Formatted: Indent: First line: 2.13 ch

Deleted:

Deleted: calculated for COD of 1 - 64 and CER of 2 – 32 µm at an interval of 1 for each solar zenith and azimuth angles of 30° and 0°, respectively by assuming cloud phase as water cloud. We assume 1% error in $lnF_0(\lambda)$, which is significantly larger than the maximum error in $lnF_0(\lambda)$ shown in Fig. 2 and discussed in section 3. This large error in $lnF_0(\lambda)$ is assumed to incorporate errors in $T(\lambda)$ generated from also other possible factors, such as radiance measurement and $\Delta\Omega(\lambda)$ estimation. Similarly, we assume surface albedo of 0.15 for all three wavelengths and PWC of 1.5 cm by assuming errors on them as ±0.025 and 1.0 cm, respectively. Though $F_0(\lambda)$ in actual data analysis is the instrument signal equivalent to the measurement performed at the top of the atmosphere (TOA), it is the incident irradiance at TOA (unit: W/m^2/nm) calculated from the radiative transfer model for error evaluation simulations discussed in this section. For each set of known COD and CER, 100 random gaussian noises for each error source mentioned above are added in the retrieval to simulate 300 sets of COD and CER. Out of them, the successful retrievals ($J \leq 3$) are used to calculate the mean bias error (MBE) as below:

$$MBE = \frac{\sum_{i=1}^{n}\left(\frac{Si}{Tr}-1\right)}{n} \quad (3),$$

where, *Si* and *Tr* represent the simulated and true values, respectively. Only the MBE is discussed here because the error map evaluated in other form, such as root mean square error (RMSE), contains the same qualitative information. Figure 3 presents MBE for COD (first column), MBE for CER (second column), and total number of successful retrieval (third column) for each type of error separately and in combination. Figures 3(a) – 3(c), 3(d) – 3(f), 3(g) – 3(i), and 3(j) – 3(l) correspond to errors in transmittance, surface albedo, PWC and all of them, respectively. The 100% unsuccessful retrieval is shown by black color. One can note that the retrieval can be more uncertain mainly when COD is less than ~15. Further, regardless of the error source, the retrieval error is relatively high especially for small (CER < ~7 µm) and large (CER > ~13 µm) cloud droplets. In general, the error domains of CER are expanded by overlapping the error domains of COD. This suggests that the error in input data can affect CER retrieval more effectively than COD retrieval. Among three different error sources, the error in transmittance can dominate the effect of remaining two error sources. The successful retrieval number corresponding to each error source shown in the third column clearly suggests two domains where the algorithm finds difficulty to fit the measurement based transmittances with modeled values. Those domains exist in ~8 < COD < ~16 with CER > ~13 µm and CER < ~7 µm. Those domains have relatively high retrieval errors as shown in the first and second columns. The relatively high errors in COD and CER are further extended for COD < ~8 despite enough number of successful retrievals. The contour lines for $T(\lambda)$ shown in Figs. 4(a), 4(b), and 4(c) for the wavelengths of 0.87, 1.02 and 1.627 µm, respectively can help to shed light for understanding those domains. The $T(\lambda)$ values shown in Figs. 4(a) – 4(c) correspond to the condition of no error in input data.

First talking about unsuccessful retrievals noted for ~8 < COD < ~16 and CER > ~13 µm domain, Figs. 4(a) - 4(c) suggest that $T(\lambda)$ values can hardly change with the increase of CER when CER > ~13 µm. As a result, the CER retrieval greater than ~13 µm is very uncertain and the retrieved CER is generally underestimated. Note that $T(\lambda)$ contour lines falling within ~8 < COD < ~16 get appear again for COD < ~2. Therefore, in an attempt of searching the best set of COD and CER by trying to fit the inputted $T(\lambda)$ values with the modeled values, the algorithm can mistakenly search the plausible solution from this small COD domain. If this happens, the retrieval may not confine

Deleted: 0

Deleted: priory

within $J \leq 3$. The algorithm is likely to compensate such underestimated CERs by overestimating CODs as clearly shown by Figs. 3(a) - 3(b) or 3(j) - 3(k).

Similarly, talking about failed retrievals for CER < ~7 µm, a very non-uniform change of *T(1.627 µm)* associated with CER change, as shown by Fig. 4(c), can be the important factor. Such very non-uniform response of CER towards *T(1.627 µm)* change can mislead the algorithm while searching the best set of COD and CER and/or may force the algorithm to mistakenly shift to COD < ~2 domain to search the plausible solution. A very careful look suggests that both CER and COD are overestimated for CER > ~7 µm. Despite enough number of successful retrieval, one can note relatively high errors in retrieved values for COD < ~8. Similar to above-discussed error domains, the retrieval errors are mainly confined for relatively large and small values of CER. It is important to note that the peak values of *T(λ)* generally fall for ~3 ≤ COD ≤ ~6. As both the forward scattering and absorption increase with the increase of COD along with the enhancement of multiple scattering, the increase in *T(λ)* before the peak value is due to the dominance of forward scattering over absorption, and opposite for the decrease in *T(λ)* after the peak value. In other words, the competition between forward scattering and absorption is maximum to increase or decrease *T(λ)* within this COD range. Not only COD, but also CER is equally important to increase or decrease *T(λ)*, and the algorithm needs to take into account of both COD and CER changes while searching the plausible set of COD and CER. Thus, it is the most sensitive COD range for the ambiguous solution of COD and CER in transmittance based remote sensing. Therefore, even a small degree of error in input data can divert both COD and CER significantly from their true values. Though weak, this phenomenon can be still active in the vicinity of this COD range to bring error in retrieved values even for COD < ~3. The weak CER response towards *T(λ)* for large CERs, as discussed above, again plays an important role to bring errors in retrieved values for relatively large CERs. At the same time, a very complicated distribution of *T(1.627 µm)* for CER < ~7 µm, as discussed above, can be an important factor for errors noted for relatively small CERs. Further, the appearance of same *T(λ)* values for larger CODs, as discussed above, can be the next important factor for errors noted within COD < ~2.

Overall speaking, the retrieval error in COD is smaller than that for CER in terms of domain coverage and error magnitude, suggesting that the transmittance based cloud remote sensing can have better effectiveness for COD retrieval than for CER retrieval. Except for a limited number of error domains discussed above, the retrieval errors are small in magnitude. For example, for COD > 15 and all types of errors, the 5, 50, and 95 percentile values of MBE for retrieved COD are -2.0%, -0.6% and 0.82%, respectively; they are -4.1%, -0.51% and 7.2%, respectively for retrieved CER. For reference, the maximum (minimum) retrieval errors for COD ≥ 20 and CER = 10 µm for a spectral method proposed by McBride et al. (2011) are ~7% (~2%) and ~52% (~14%) for COD and CER, respectively. Below, section 5 further sheds light on the quality of retrieved cloud properties based on comparison with standard data obtained from independent sources.

5 Comparison with data from independent sources

5.1 Solar radiation data

Formatted: Indent: First line: 2.13 ch

Deleted:

Deleted: ~~Note that the absorption tends to reduce *T(λ)*, whereas the forward scattering tends to increase it.~~

Formatted: Strikethrough

Deleted: error

Deleted: values

Deleted: compassion

The broad-band radiance and irradiance of shortwave spectral range (0.3 – 2.8 μm) observed at Chiba (35.62°N,140.10°E) at each 20 seconds from December 2015 to December 2016 using a narrow-angle (NA) radiometer (FOV: 5°) and a pyranometer (FOV: 180°), respectively are used for the evaluation of sky radiometer observed cloud properties. The broad-band irradiance and broad-band radiance of spectral range mentioned above are observed by instruments manufactured by Kipp and Zonen, Netherland and EKO Instruments Co., Ltd., Japan, respectively. The latter can observe the downwelling irradiance signals in terms of voltage at a very narrow FOV. The instrument was calibrated by a manufacturer in the laboratory, and by using such calibration constant value, it is possible to convert the observed signals into radiance of unit $W/m^2/sr$. As the sensor faces upward and the instrument's FOV is narrow, the signal measured by this instrument can be regarded as the downwelling radiance of zenith direction. The cloud properties from the sky radiometer are combined with MODIS observed surface albedo and radiosonde observed PWC to calculate the counterparts of observation. A comparison is done for an average of 5 minutes observation of solar radiation that centers the sky radiometer observation time. Figures 5(a) and 5(b) show the comparison for broad-band radiance and irradiance, respectively. For reference, such comparison is done also for modeled values using cloud properties of AHI instead of sky radiometer. They are shown in Figs. 5(c) and 5(d) for broad-band radiance and irradiance, respectively.

Formatted: Superscript

Firstly, one can see a strong (weak) correlation between modeled and observed values for broad-band radiance (irradiance) when cloud properties from sky radiometer are used. One the other hand, the correlation between modeled and observed values for broad-band radiance (irradiance) are weak (strong) for AHI cloud properties. Rather than pyranometer, the NA radiometer observed data can best describe the quality of sky radiometer cloud properties because of narrow FOV. A very good agreement noted in Fig. 5(a) with correlation coefficient (*r*) as strong as 0.93 suggests that sky radiometer based cloud properties (at least COD) are qualitative enough. As the contribution of COD is dominant over CER in broad-band solar radiation (Khatri et al., 2018), Fig. 5(a) alone cannot justify the quality of retrieved CER. At the same time, the relatively poor agreement for irradiance comparison shown in Fig. 5(b) can be described due to significantly different FOV of sky radiometer and pyranometer. It is because the surface observed solar radiation can be drastically different depending on the instrument FOV. As an example, Fig. 6 shows the scatter plot between broad-band irradiance and radiance observed by pyranometer and NA radiometer, respectively at Chiba during January – March , 2016. The correlation between them is very poor. One of the important factors that deteriorates the correlation between them is the cloud horizontal inhomogeneity. This can plausibly explain the poor agreement in Fig. 5(b) despite reasonably accurate retrieval from the sky radiometer as evidenced by Fig. 5(a). On the contrary, AHI cloud properties are average (or representative) values of specific coverage, i.e., pixel (e.g., 1km x 1km). As a result, irradiances modeled from AHI cloud properties become closer with observed irradiance than those modeled from sky radiometer cloud properties. It is because the sky radiometer observed cloud can be just a small portion of a pixel containing horizontally inhomogeneous clouds.

Deleted: highly

5.2 Satellite cloud products

As part of validating water cloud products of MODIS and AHI using surface radiation data, Khatri et al. (2018) compared water cloud properties retrieved from sky radiometer with those of MODIS and AHI observations for three observation sites of SKYNET: Chiba, Hedo-misaki, and Fukue-jima for the period of October, 2016 to December, 2017. They further used surface irradiance data, and found that the validation results using sky radiometer and surface irradiance data are qualitatively same. A fairly good (poor) agreement was shown for COD (CER) between sky radiometer and satellite products in Khatri et al. (2018). They compared sky radiometer results with results of collocated satellite pixels by selecting samples with time difference less than 1.25 minutes, which is half of temporal resolution of AHI observation over Japan, and the distance between the pixel center and the observation site less than 1 km, and further doing parallax correction for satellite products.

It is learnt from section 5.1 that the inhomogeneous clouds and/or broken clouds contained within the satellite pixels are major obstacles in quality assessment of satellite products using sky radiometer results and vice versa. This section attempts to improve our understating regarding the quality of sky radiometer products by using satellite products effectively. For this purpose, we prepare samples for the comparison by addressing the cloud inhomogeneity related problem in a logical way with available information at hand. If surface irradiance calculated from sky radiometer cloud properties agree well with that observed at surface, the effective COD of actual inhomogeneous clouds may be represented by a sky radiometer COD. Here, effective COD refers to COD of assumed plane-parallel homogenous cloud layers which can produce irradiance equivalent to that produced by actual inhomogeneous clouds, i.e., measured irradiance. Note that the satellite cloud properties retrieved from reflected signals assume clouds as plane-parallel homogenous layers. The sky radiometer cloud properties that generate surface irradiances equivalent to observed values by differing not more than 1% are selected to compare with satellite cloud properties. Figures 7(a) and 7(b) show the comparison of sky radiometer CODs with MODIS and AHI values, respectively for sites and period same to Khatri et al. (2018). The COD agreement is fairly good. The results are qualitatively same for both MODIS and AHI, by showing r values of ~0.6 and ~0.7 and RMSE values of ~13 and ~10 for MODIS and AHI, respectively. Despite several differences between sky radiometer and satellite products from both observation and retrieval perspectives, a fairly good agreement indicates that they can have similar response towards thin and thick clouds, though the COD value may not be exactly same. Similarly, Figs. 8(a) and 8(b) show the comparison of sky radiometer CERs with MODIS and AHI values, respectively. The water absorbing wavelengths corresponding to MODIS and AHI are 2.1 μm and 3.79 μm, respectively. The CERs between sky radiometer and satellite sensors are poorly correlated. One can see r less than 0.12 and RMSE of ~7 μm for both satellite sensors. Such a poor correlation can be mainly due to the fact that satellite sensors using reflected signals are highly sensitive towards cloud top layers (Platnick, 2000), whereas the sky radiometer is sensitive to whole cloud layers.

Though qualitive information revealed from Khatri et al. (2018) and comparison results of Figures 7 and 8 of this study are in general the same, there are some differences in Figures 7 and 8 with respect to comparison plots shown in Khatri et al. (2018). Application of data screening criteria as mentioned above generally screened out those data that had considerably large difference between sky radiometer and satellite sensors. Such large difference in the previous

Deleted:

Deleted: 6

Deleted: 6

Deleted: 7

Deleted: 7

comparison was likely due to different FOVs of satellite sensor and sky radiometer while observing inhomogeneous clouds. Thus, the comparison results presented in this study by addressing such cloud inhomogeneity related problem more logically is expected to give more accurate and refined information than those presented in Khatri et al. (2018).

Deleted:

6 Conclusions

In an effort of making cloud observation from surface more common and convenient, this study develops an algorithm to retrieve cloud properties (COD and CER) from spectral zenith radiances measured by sky radiometer. By taking into account of a priori information of a state vector and errors related to observation based transmittance and used ancillary data (PWC and surface albedo), an optimal-estimation approach is proposed by fitting observation based transmittances at the wavelengths of 0.87, 1.02, and 1.627μm with modeled values. To further ease data analysis of long-term observation by overcoming the filter degradation problem, an on-site method of calibration for direct intensity is proposed by making use of aerosol data of very clear sky days. The calibration constants derived from the proposed method agree quite well with values determined by collocating the field instruments with the master instrument. The retrieval error analyses performed by considering known ranges of errors in observation based transmittances and ancillary data suggest a good performance of the algorithm, except for a certain narrow bands of small COD and CER values. In general, the errors in input information can affect CER retrieval more significantly than COD retrieval, and the retrieved CER can have relatively large errors when clouds are optically thin (COD < ~15) and cloud droplets are small (CER < ~7 μm) or large (CER > ~13 μm) in size. As part of quality assessment, cloud properties retrieved from the proposed algorithm are compared indirectly with surface observed radiance/irradiance data and directly with MODIS and AHI observed cloud properties. The retrieved cloud properties are found to produce the broadband shortwave radiances quite similar to those observed by a narrow-angle radiometer, confirming the good quality of retrieved products (at least COD) from sky radiometer. However, the agreement is relatively poor when broadband shortwave irradiances observed by a pyranometer of wide FOV are compared with the modeled values. It is likely due to distinctly different FOVs of sky radiometer and pyranometer, suggesting a very important influence of instrument's FOV on cloud remote sensing. Further, a fairly good agreement of COD between sky radiometer and satellite sensors can be seen; however, the agreement is poor for CER comparison.

Code/Data Availability: Data and retrieval code are available from the corresponding author upon request.

Author Contribution: PK, HI, and TH developed study framework and code. HI, TT, AY, and AD generated data. HL and QK helped in advancing study framework and manuscript writing. All co-authors read the manuscript and provided suggestions and comments.

Competing interests: The authors declare that they have no conflict of interest.

Acknowledgements: This research is supported by the 2nd Research Announcement on the Earth Observations of the Japan Aerospace Exploration Agency (JAXA) (PI No. ER2GCF211, Contract No. 19RT000370), a Grant-in-Aid for Scientific Research (C) 17K05650 from Japan Society for the Promotion of Science (JSPS), "Virtual Laboratory for Diagnosing the Earth's Climate System" program of MEXT, Japan, and CREST/JST research fund of grant number JPMJCR15K4.

References

Campanelli, M., Nakajima,T., and Olivieri, B.: Determination of the solar calibration constant for a sun-sky radiometer: Proposal of an in situ procedure, Appl. Opt., 43(1), 651–659, https://doi.org/10.1364/AO.43.000651, 2004.

Campanelli, M., Nakajima, T., Khatri, P., Takamura, T., Uchiyama, A., Estelles, V., Liberti, G. L., and Malvestuto: Retrieval of characteristic parameters for water vapour transmittance in the development of ground based sun-sky radiometric measurements of columnar water vapour, Atmos. Meas. Tech., 7, 1075-1087, https://doi.org/10.5194/amt-7-1075-2014, 2014.

Chiu, J. C., Huang, C.-H., Marshak, A., Slutsker, I., Giles, D. M., Holben, B. N., Knyazikhin, Y., and Wiscombe, W. J: Cloud optical depth retrievals from the Aerosol Robotic Network (AERONET) cloud mode observations, J. Geophys. Res., 115, https:/doi.org/10.1029/2009JD013121, 2010.

Chiu, J. C., Marshak, A., Huang, C.-H., Varnai, T., Hogan, R. J., Giles, D. M., Holben, B. N., O'Connor, E. J., Knyazikhin, Y., and Wiscombe, W. J.: Cloud droplet size and liquid water path retrievals from zenith radiance measurements: examples from the Atmospheric Radiation Measurement Program and the Aerosol Robotic Network, Atmos. Chem. Phys., 12(8), 10313–10329, https://doi.org/10.5194/acp-12-10313-2012, 2012.

Forster, P., Ramaswamy, V., Artaxo, P., Berntsen, T., Betts, R., Fa- hey, D. W., Haywood, J., Lean, J., Lowe, D. C., Myhre, G., Nganga, J., Prinn, R., Raga, G., Schulz, M., and Van Dorland, R.: Changes in Atmospheric Constituents and in Radiative Forc- ing, in: Climate Change 2007: The Physical Science Basis, con- tribution of Working Group I to the Fourth Assessment Report of the Intergovernmental Panel on Climate Change, edited by: Solomon, S. D., Qin, M., Manning, Z., Chen, M., Marquis, K. B., Averyt, M. T., and Miller, H. L., Cambridge University Press, Cambridge, United Kingdom and New York, NY, USA, 129– 134, 2007.

Hashimoto, M., Nakajima T., Dubovik, O., Campanelli, M., Che, H., Khatri. P., Takamura, T., and Pandithurai, G.: Development of a new data-processing method for SKYNET sky radiometer observations, Atmos. Meas. Tech., 5, 5, 2723-2737, https://doi.org/10.5194/amt-5-2723-2012, 2012.

Khatri, P. and Ishizaka,Y.: Effects of Continentally Polluted Air Mass on Aerosol Optical Properties over the East China Sea, J. Meteor. Soc. Japan, 85(1), 47-68, https://doi.org/10.2151/jmsj.85.47, 2007.

Khatri, P., Takamura, T., Yamazaki, A., and Uchiyama, A.: Use of 315nm channel data of sky radiometer to estimate columnar ozone concentration: A preliminary study J. Meteor. Soc. Japan, 92A, 185-194, https://doi.org/10.2151/jmsj.2014-A12, 2014.

Khatri, P., Takamura, T., Estellés, V., Irie, H., Kuze, H., Campanelli, M., Sinyuk, A., Lee, S.-M., Sohn, B. J., Pandithurai, G., Kim, S.-W., Yoon, S. C., Martinez-Lozano, J. A., Hashimoto, M., Devara, P. C. S., and Manago, N.: Factors for inconsistent aerosol single scattering albedo between SKYNET and AERONET, J. Geophys. Res., 121(4), 1859-1877, https:/doi.org/10.1002/20159JD023976, 2016.

Khatri, P., Hayasaka, T., Iwabuchi, H., Takamura, T., Irie, H., and Nakajima, T. Y.: Validation of MODIS and AHI observed water cloud properties using surface radiation data, J. Meteor. Soc. Japan, 96B, 151-172, https:/doi.org/10.2151/jmsj.2018-036, 2018.

Kikuchi, N., Nakajima, T., Kumagai, H., Kuroiwa, H., Kamei, A., Nakamura, R., and Nakajima, T. Y.: Cloud optical thickness and effective particle radius derived from transmitted solar radiation measurements: Comparison with cloud radar observations, J. Geophys. Res., 111, https:/doi.org/10.1029/2005JD006363, 2006.

King, M. D., Byrne, D. M., Herman, B. M., and Reagan, J. A.: Aerosol Size Distributions Obtained by Inversion of Spectral Optical Depth Measurements, J. Atmos. Sci., 35, 2153–2167, https://doi.org/10.1175/1520-0469(1978)035%3C2153:ASDOBI%3E2.0.CO;2, 1987.

LeBlanc, S. E., Pilewskie, P., Schmidt, K. S., and Coddington, O.: A spectral method for discriminating thermodynamic phase and retrieving cloud optical thickness and effective radius using transmitted solar radiance spectra, Atmos. Meas. Tech., 8, 1361-1383, https://doi.org/10.5194/amt-8-1361-2015, 2015.

McBride, P. J., Schmidt, K. S., Pilewskie, P., Kittelman, A. S., and Wolfe, D. E.: A spectral method for retrieving cloud optical thickness and effective radius from surface-based transmittance measurements, Atmos. Chem. Phys., 11, 7235–7252, https://doi.org/10.5194/acp-11-7235-2011, 2011.

Nakajima, T. and King, M. D.: Determination of the optical thickness and effective particle radius of clouds from reflected solar radiation measurements. Part I: Theory, J. Atmos. Sci., 47, 1878–1893, https://doi.org/10.1175/1520-0469(1990)047%3C1878:DOTOTA%3E2.0.CO;2, 1990.

Nakajima, T., Tonna, G., Rao, R., Kaufman, Y., and Holben, B. N. : Use of sky brightness measurements from ground for remote sensing of particulate polydispersions, Appl. Opt., 35(15), 2672–2686, https://doi.org/10.1364/AO.35.002672, 1996.

Platnick, S. : Vertical photon transport in cloud remote sensing problems, J. Geophys. Res., 105, 22919–22935, https://doi.org/10.1029/2000JD900333, 2000.

Rodgers, C. D.: Inverse Methods for Atmospheric Sounding: Theory and Practice (Vol. 2), Ser. Atmos. Oceanic Planet. Phys., 2, World Sci., Hackensack, NJ, 2000.

Ricchiazzi, P., Yang, S., Gautier, C., and Sowle, D.: SBDART: A research and teaching software tool for plane-parallel radiative transfer in the Earth's atmosphere, Bull. Am. Meteorol. Soc., 79, 2101-2114, https://doi.org/10.1175/1520-0477(1998)079%3C2101:SARATS%3E2.0.CO;2, 1998.

Rosenfeld, D., Andreae, M. O., Asmi, A., Chin, M., de Leeuw, G., Donovan, D., Kahn, R., Kinne, S., Kivekäs, N., Kulmala, M., Lau, W., Schmidt, S., Suni, T., Wagner, T., Wild, M., and Quaas, J.: Global observations of aerosol-cloud-precipitation-climate interactions, Rev. Geophys., 52, 750–808, https://doi.org/10.1002/2013RG000441, 2014.

Figures

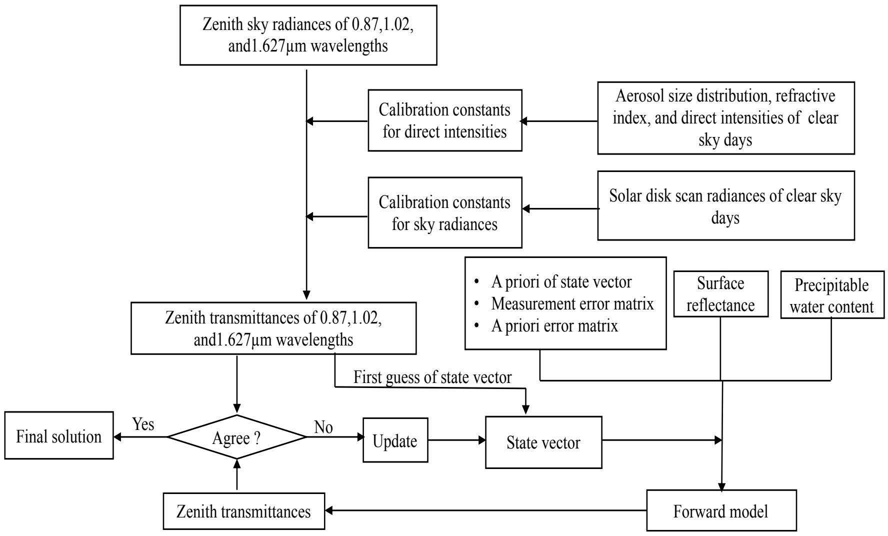

Figure 1: A schematic diagram of study method.

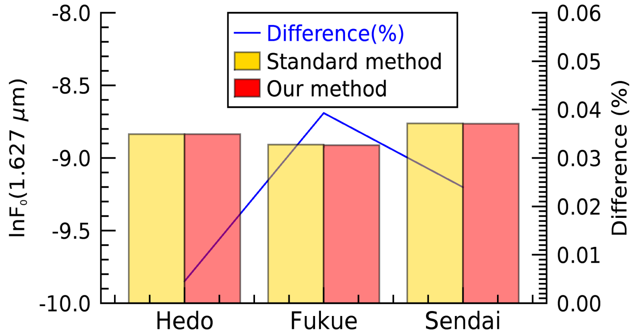

Figure 2: Comparison of direct intensity calibration constant (lnF$_0$) values at water absorbing wavelength of 1.627 μm between the standard method (calibration using the master instrument) and an on-site method proposed in this study for sky radiometers belonging to Hedo-misaki (26.87°N, 128.25°E), Fukue-jima (32.75°N, 128.68°E), and Sendai (38.26°N,140.84°E). Shown in the figure is also the difference (%), i.e., the difference (in percentage) between proposed method and the standard method normalized by the value of the standard method.

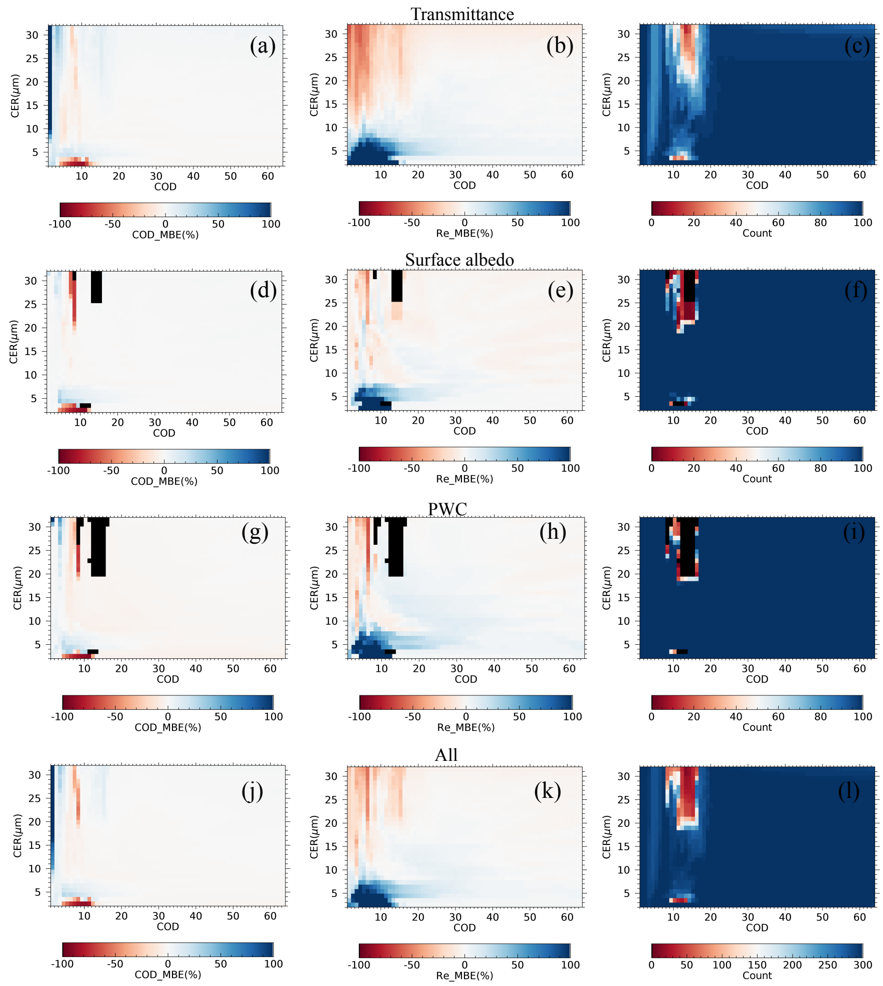

Figure 3: Mean bias error (MBE) values for retrieved COD and CER and total number of successful retrieval in (a), (b) and (c), respectively for assumed error in transmittance; (d) – (f): same as upper panel but for assumed error in surface albedo; (g) – (i): same as upper panel but for assumed error in precipitable water content; (j) – (l): same as upper panel but for all error sources. The 100% unsuccessful retrieval is denoted by black color.

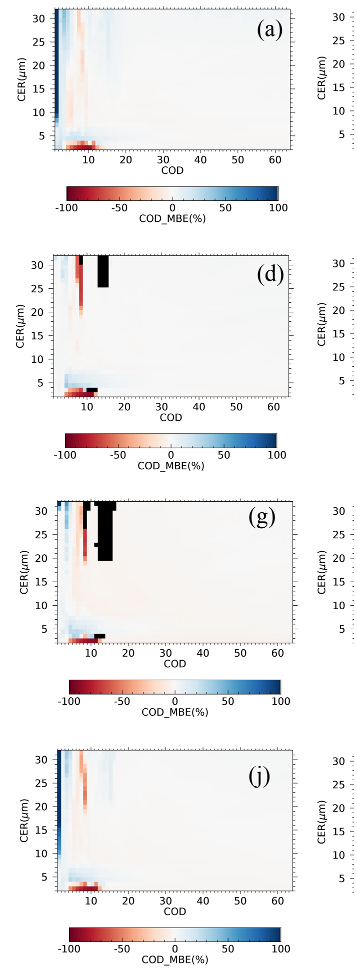

Deleted:

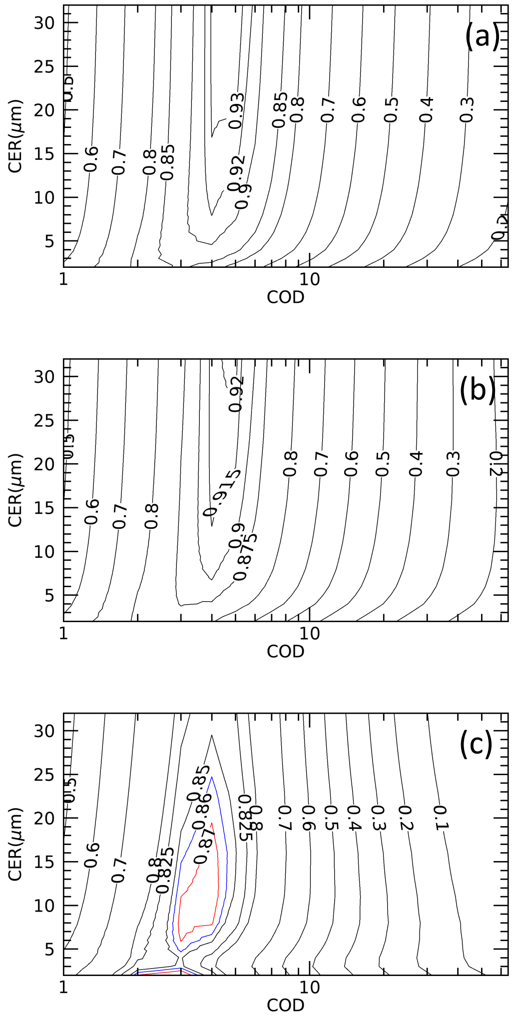

Figure 4: Contour plots of transmittances at the wavelengths of (a) 0.87 µm, (b) 1.02 µm, and 1.627 µm for solar zenith and azimuth angles of 30° and 0°, respectively. The values of transmittances are given within the contour lines. Different colors are used for 1.627 µm to make it easy to distinguish.

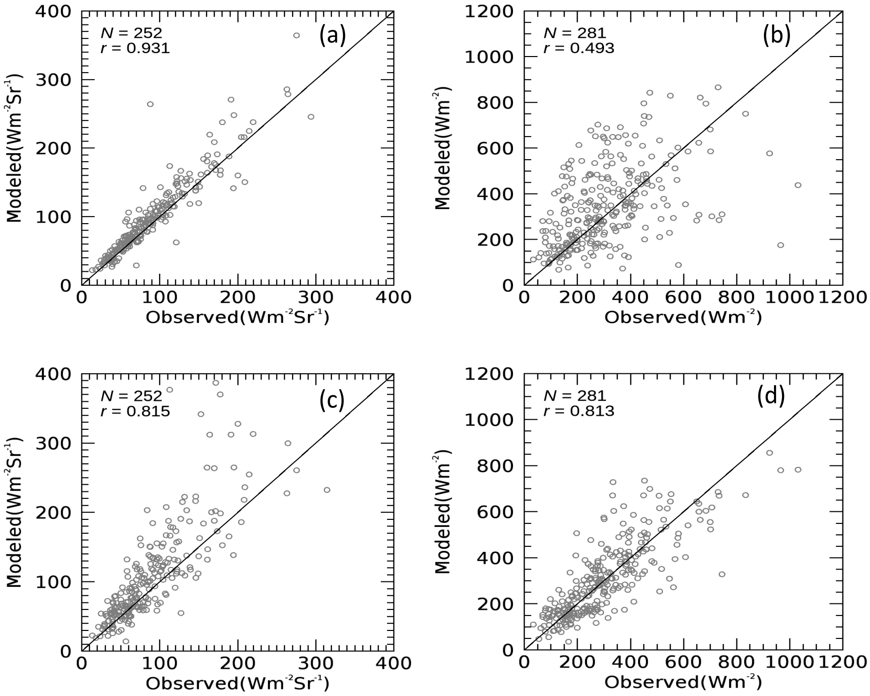

Figure 5: Comparison between modeled and observed broad-band (a) radiances and (b) irradiances for modeled values using sky radiometer cloud proprieties for observation site of Chiba (35.62°N,140.10°E) for 2016. Similarly, (c) and (d) show the comparison results for broad-band radiances and irradiance, respectively for modeled cloud properties corresponding to AHI.

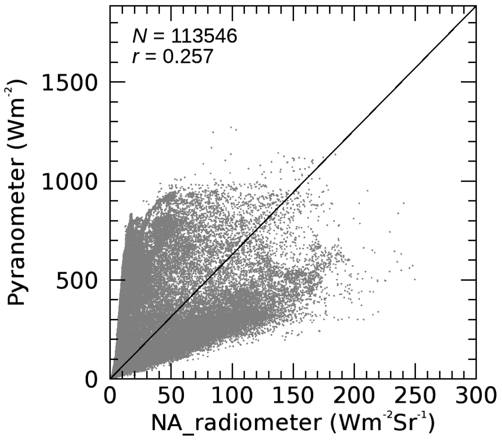

Figure 6: Scatterplot of broad-band radiances and irradiances observed by radiometers of narrow-angle and wide-angle (pyranometer), respectively at Chiba (35.62°N,140.10°E) during January – March, 2016. A solid line represents a straight line for $y = 2\pi x$.

Deleted:

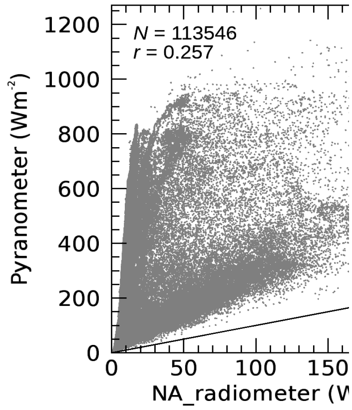

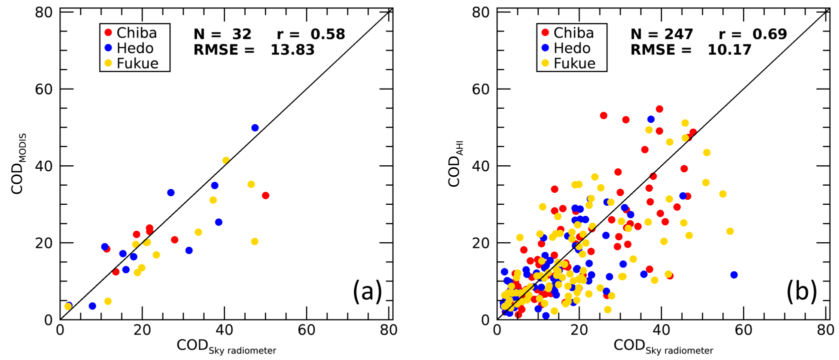

Figure 7: Comparison of sky radiometer CODs with (a) MODIS and (b) AHI CODs for observation sites of Chiba (35.62°N,140.10°E), Hedo-misaki (26.87°N, 128.25°E), Fukue-jima (32.75°N, 128.68°E) for periods of October, 2015 to December, 2016.

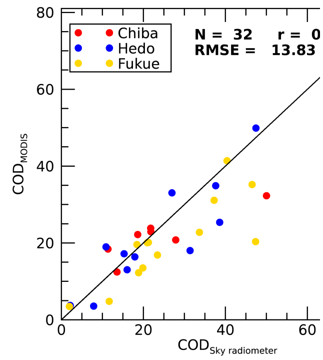

Deleted:

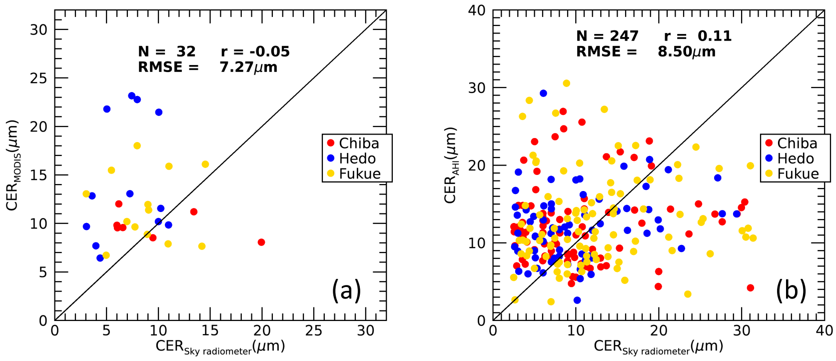

Figure 8: Same as Figure 7, but for CER comparison.

Deleted:

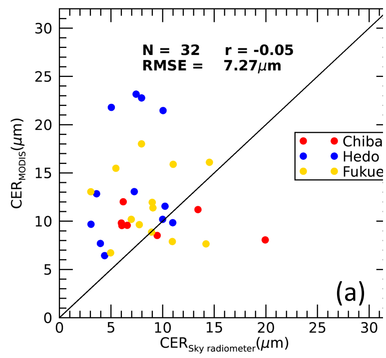

Changes made during English correction by a professional proof reader

Retrieval of cloud properties from spectral zenith radiances observed by sky radiometers

Abstract: An optimal estimation algorithm to retrieve cloud optical depth (COD) and cloud particle effective radius (CER) from spectral zenith radiances observed by narrow field-of-view (FOV) ground-based sky radiometers is developed. To address the filter degradation problem further by analyzing long-term observation data, an on-site calibration procedure is proposed, which has good accuracy compared with the standard calibration transfer method. An error evaluation study conducted by assuming errors in observed transmittances and ancillary data for water vapor concentration and surface albedo suggests that the errors in input data affect retrieved CER more than COD. Except for some narrow domains that fall within COD < 15, the retrieval errors are small for both COD and CER. The retrieved cloud properties reproduce the broadband radiances observed by a narrow FOV radiometer more precisely than broadband irradiances observed by a wide FOV pyranometer, justifying the quality of the retrieved product (at least COD) and indicating the important effect of the instrument FOV in cloud remote sensing. Furthermore, CODs (CERs) from sky radiometer and satellite observations show good (poor) agreement.

1 Introduction

Clouds play an important role in driving the climate system and hydrological cycle (Rosenfeld et al., 2014). The accurate representation of clouds in the global climate model remains one of the largest uncertainties (Forster et al., 2007). Clouds are observed from space with various sensors onboard satellites, and the observations are vital in understanding more about cloud characteristics and their roles in the climate system and hydrological cycle. The quality assurance of cloud properties from satellite observations is an important task in cloud remote sensing, although it is challenging, primarily due to the lack of standard data representing different atmospheric conditions. Compared with the routine observation of aerosols through surface networks, such as AERONET (https://aeronet.gsfc.nasa.gov/) and SKYNET (http://atmos3.cr.chiba-u.jp/skynet/), observation of clouds from the surface is performed at a limited number of stations, and most of the observation data are not easily accessible. The cloud observations from multiple stations in ground-based networks around the world could be improved because their instruments for aerosol observation are also suitable for cloud observation [[Please confirm.]]. These observations will help the satellite remote sensing community to validate cloud products and help the whole cloud research community to study clouds in more detail by using high-resolution surface data.

Clouds have been studied from the surface by using zenith radiances observed by radiometers belonging to AERONET (e.g., Chiu et al., 2010, 2012) and SKYNET (e.g., Kikuchi et al., 2006). In accordance with the literature, the AERONET and SKYNET radiometers are referred to as sun photometers and sky radiometers, respectively. Similar to space-based cloud remote sensing using reflected signals (e.g., Nakajima and King, 1990), studies using sun photometer and sky radiometer data use a look-up-table (LUT). The fundamental idea is to compare the observed signals with LUT data corresponding to prior known cloud optical depth (COD) and cloud particle effective radius (CER) while finding a

Deleted: sky radiometer observed

Deleted: -…estimation based …lgorithm to retrieve cloud optical thickness …epth (COD) and cloud -…article effective radius (CER) from spectral zenith radiances observed by a …arrow field …of …view (FOV) ground-based sky radiometers is developed. To further …ddress the filter -…egradation problem further while …y analyzing data of …ong-term observation data, an on-site calibration procedure is proposed, which is found to have a very…as good accuracy with respect to…ompared with a …he standard procedure, i.e., a …alibration transfer method. An error evaluation study conducted by assuming errors in observeation-base… transmittances and ancillary data of for water vapor concentration and surface albedo suggests that the errors in input data can influence…ffect retrieved CER more effectively …han COD. Except for some narrow domains that fall within COD < 15, the retrieval errors are very…small for both COD and CER. The retrieved cloud ... [1]

Deleted: to …n drive …riving the climate system and hydrological cycle (Rosenfeld et al., 2014). Their…accurate representation of clouds in the global climate model remains ... [2]

Formatted ... [3]

Deleted: of …ultiple stations of …n above-mentioned ground-based networks around the world, …cloud observations from them should ... [4]

Formatted: Highlight

Deleted: strengthen

Formatted: Highlight

Deleted: as …ecause their operating …nstruments for aerosol observation are also capable …uitable for cloud observation as well…[[Please confirm.]]. This …hese ... [5]

Deleted: It is important to mention that efforts have been made in the past for studying c…louds have been studied from the surface by using zenith radiances observed by ... [6]

plausible solution for the COD and CER combination. This signal can be zenith radiance or transmittance. Chiu et al. (2010) retrieved COD from a LUT of zenith radiances of water non-absorbing wavelengths constructed by assuming a fixed CER, and Chiu et al. (2012) and Kikuchi et al. (2006) used a LUT of transmittances of water non-absorbing and absorbing wavelengths to infer COD and CER simultaneously. The reflected signals for water non-absorbing and absorbing wavelengths can have nearly one-to-one relationships with COD and CER, respectively. On the other hand, transmitted signals do not behave in this manner, making the retrieval process difficult for a LUT approach using transmitted signals. In addition, unlike reflected signals, transmitted signals are weakly sensitive to changes in CER. This makes retrieval using transmitted signals more complex. Furthermore, the shape of the LUT may change depending on the solar position, making the retrieval process even more cumbersome if LUTs developed for a limited number of specific solar positions are used. To overcome these difficulties, some innovative techniques have been proposed. For example, McBride et al. (2011) developed a spectral method by using the slope of the transmittances of 13 wavelengths between 1565 and 1634 nm and the transmittance at the visible wavelength of 515 nm to retrieve COD and CER simultaneously. LeBlanc et al. (2015) derived 15 parameters to quantify spectral variations in shortwave transmittances due to absorption and scattering of liquid water and ice clouds, manifested by shifts in spectral slopes, curvatures, maxima, and minima, to discriminate cloud phase and retrieve COD and CER. However, these techniques were developed for radiometers with high spectral resolution and are less suitable for sun photometers and sky radiometers because they have a limited number of channels.

Here, we develop a retrieval algorithm based on an optimal estimation method, namely, a maximum a posteriori method (Rodgers, 2000). We use three carefully selected wavelengths to retrieve COD and CER simultaneously. An on-site calibration method is proposed to address the filter degradation problem while analyzing long-term observation data. Although the algorithm is developed using sky radiometer data, it is equally applicable for sun photometer data. The paper begins with a brief description of the sky radiometer in Section 2. The methodology, retrieval error, and quality assessment of retrieved products are discussed in Sections 3–5, respectively. Finally, the conclusion is presented in Section 6.

2 Sky radiometer

The sky radiometer (POM-02, PREDE Co. Ltd., Japan) can make observations of direct intensity, angular sky radiance (both almucantar and principle plane scans), and zenith sky radiance at 11 wavelengths at specified time intervals. The field of view (FOV) is 1°. The most commonly used wavelengths by SKYNET are 0.315, 0.34, 0.38, 0.4, 0.5, 0.675, 0.87, 0.94, 1.02, 1.627, and 2.2 µm. The direct and angular sky radiances at wavelengths of 0.34, 0.38, 0.4, 0.5, 0.675, 0.87, and 1.02 µm, at which the absorptions by atmospheric gases and water/ice are negligible, are used for aerosol remote sensing (Nakajima et al., 1996; Hashimoto et al., 2012). The direct intensities observed at wavelengths of 0.315 and 0.94 µm are used for remote sensing of ozone (Khatri et al., 2014) and water vapor (e.g., Campanelli et al., 2014), respectively. The zenith sky radiances have different potential applications. The zenith sky radiances of cloudy skies have been used for cloud remote sensing (e.g., Kikuchi et al., 2006). The calibration constant terms for sky radiance (angular and zenith)

Deleted: ; … and Chiu et al. (2012) and Kikuchi et al. (2006) used a LUT of transmittances of water non-absorbing and absorbing wavelengths to infer COD and CER simultaneously. It is important to note that t…he reflected signals for water non-absorbing and absorbing wavelengths can have nearly one-to-one relationships with COD and CER, respectively. On the other hand, transmitted signals do notsuch…behaviors cannot be seen for… in this manner transmitted signals… making the retrieval process very…difficult for a LUT based …pproach using transmitted signals. In addition, unlike reflected signals, the …ransmitted signals is …re weakly sensitive to changes in CER change. ... [7]

Deleted: Taking above-mentioned…ere, difficulties in mind, we develop …e develop a retrieval algorithm based on an optimal-…estimation method, i.e.…amely, a maximum a posteriori (MAP) …ethod (Rodgers, 2000). We use three carefully selected wavelengths to retrieve COD and CER simultaneously. Further, a…n on-site calibration method is proposed to cope …ddress the filter degradation problem while analyzing data of …ong-term observation data. Though …lthough the algorithm is developed by …sing data of …ky radiometer data, it is equally applicable for data of sun photometer data. ... [8]

Deleted: Model: …OM-02,), manufactured by…PREDE Co. Ltd., Japan),…is an instrument capable to…an make observations of direct intensity, angular sky radiance (both almucantar and principle plane scans), and zenith sky radiance at 11 wavelengths at specified time intervals. The field of view (FOV) is 1°. The most commonly used wavelengths by SKYNET are 0.315, 0.34, 0.38, 0.4, 0.5, 0.675, 0.87, 0.94, 1.02, 1.627, and 2.2 µm. Among them, t…he direct and angular sky radiances at the …avelengths of 0.34, 0.38, 0.4, 0.5, 0.675, 0.87, and 1.02 µm, at which the absorptions by atmospheric gases and water/ice are ... [9]

and direct intensity are required while deriving physical data from observation signals via retrieval algorithms. One of the largest benefits of the PREDE sky radiometer is that these calibration constants can be obtained from field observation data, as outlined by Nakajima et al. (1996). In brief, an improved Langley (IL) method (Nakajima et al., 1996; Campanelli et al., 2004), which is an alternative to the normal Langley (NL) method, can be used to obtain calibration constants for direct intensities. Similarly, the solar disk scan method, which is an alternative to integrating sphere methods, can be used to determine the calibration constant for sky radiances. A more detailed study of sky radiometers and their calibration can be found in Khatri et al. (2016).

3 Methodology

A schematic of the study method is shown in Figure 1. We use sky radiances (E) observed at three longer wavelengths (0.87, 1.02, and 1.627 µm), excluding 2.2 µm, which is not used for two main reasons. First, our statistical analysis suggests that the number of unphysical data (observation data recorded as 0) for 2.2 µm is high; thus, 2.2 µm is excluded to increase the retrieval number. Second, the longest wavelength used by AERONET as 1.64 µm, so the proposed algorithm could be used for sun photometer observed data as well. Wavelengths shorter than 0.87 µm are not used to avoid the effect of aerosols as far as possible. Observed E can be converted to the transmittance (T) by

$$T(\lambda) = \frac{\pi E(\lambda)}{\mu_0 \Delta\Omega(\lambda) F_0(\lambda)}, \tag{1}$$

where μ_0 is the cosine of the solar zenith angle, $\Delta\Omega$ is the calibration constant for sky radiance, which is also called the solid view angle by the SKYNET community, F_0 is the calibration constant for direct intensity, and λ is the wavelength. $\Delta\Omega$ for 0.87, 1.02, and 1.627 µm can be determined from the solar disk scan during clear sky days (Nakajima et al., 1996). Although the current IL method can be used to determine temporal F_0 for the first two wavelengths (0.87 and 1.02 µm), it is less suitable for water absorbing wavelengths, such as 1.627 µm. For 1.627 µm, F_0 derived from the NL method can be used, but NL is less practical to use routinely in short time intervals (e.g., each month) to derive temporal F_0. We prefer to use temporal F_0 for all wavelengths to include filter degradation with time (e.g., Khatri et al., 2014). To derive temporal F_0 at 1.627 µm, we use an alternative IL method, as proposed by Khatri et al. (2014). In brief, aerosol data (refractive index and volume size distribution) and direct intensity observed at 1.627 µm ($F_{1.627}$) are used. Aerosol optical thickness (τ_{aer}) depends primarily on aerosol size distribution, and the refractive index makes a small contribution to τ_{aer} (King, 1978; Khatri and Ishizaka, 2007). Thus, the refractive index at 1.02 µm, which is the highest wavelength for routine aerosol retrieval, is assumed to be the same as for 1.627 µm while calculating τ_{aer} at 1.627 µm from the volume size distribution using a Mie calculation. The optical air mass (m) and sun-earth distance (R) are calculated from the latitude and longitude of the observation site and time. Similarly, the Rayleigh scattering optical depth at 1.627 µm ($\tau_{Ray,1.627}$), though small in magnitude, is calculated from the atmospheric pressure of the observation site. Finally, the Beer–Lambert law, $\ln(F_{1.627}R^2) = \ln F_{0,1.627} - (\tau_{aer} + \tau_{Rayleigh})m$ is used to determine $\ln F_{0,1.627}$, which is the natural logarithm of the calibration constant of the direct intensity at 1.627 µm. This is calculated using data for all clear sky periods of each month to correlate $\ln(F_{1.627}R^2)$ with $(\tau_{aer} + \tau_{Rayleigh})m$. The outlier that decreases the correlation most is detected and

Deleted: those …hese calibration constants can be obtained from field observation data, themselves …s outlined by Nakajima et al. (1996). In brief, an iI…proved Langley (IL) method (Nakajima et al., 1996; Campanelli et al., 2004), which is an alternative of …o the Normal …ormal Langley (NL) method, can be used to obtain calibration constants for direct intensities. Similarly, the solar disk scan method, ... [10]

Deleted: The … schematic diagram …f the study method is ... [11]

Formatted: Font: Italic

Deleted: . The longest wavelength of 2.2 µm… which is not ... [12]

Formatted ... [13]

Deleted: the equation below:

Deleted: termed as…alled the solid view angle in ... [14]

Formatted: Font: Not Italic

Formatted ... [15]

Deleted: those three wavelengths….87, 1.02, and 1.627 µm ... [16]

Formatted ... [17]

Deleted: be conducted…se routinely within ... [18]

Formatted ... [19]

Deleted: take into account…nclude of…filter degradation ... [20]

Deleted: Note that a

Formatted: Font: Not Italic

Formatted: Font: Not Italic

Deleted: has …akes a very ... [21]

Formatted: Font: Not Italic

Deleted: the wavelength of

Formatted: Font: Not Italic

Deleted: observation …ime. Similarly, the Rayleigh- ... [22]

Formatted: Font: Not Italic

Deleted: very…small in magnitude, is calculated from the ... [23]

Formatted ... [24]

Deleted: i.e., …hich is the natural logarithm of the ... [25]

Formatted ... [26]

Deleted: deteriorates …ecreases the correlation utmost ... [27]

removed in each iteration until the condition of the correlation coefficient ($r \geq 0.997$) is satisfied. To understand the quality of the ln $F_{0,1.627}$ values calculated with this method, we compare them with data from an independent standard method. In the standard method, a calibration constant is derived by performing collocated observations with field and master instruments. Figure 2 compares ln $F_{0,1.627}$ for three different sky radiometers at the observation sites of Hedo-misaki (26.87°N, 128.25°E), Fukue-jima (32.75°N, 128.68°E), and Sendai (38.26°N,140.84°E). There is good agreement between our method and the standard method for all three sky radiometers. The relative difference (percentage), defined as the difference between our method and the standard method normalized by the value of the standard method, is also shown, and is less than 0.05% for all sky radiometers. This confirms the validity of our proposed method, which is inexpensive and easy. Thus, the proposed method can be used to determine temporal variation of ln $F_{0,1.627}$, which is useful for analyzing long-term observation data by mitigating the filter degradation problem. By using the volume size distribution and refractive indices of the wavelengths, the proposed method can be used for 0.87 and 1.02 µm as well. There is negligible difference in the values obtained by the IL method and this method for the first two wavelengths. This study uses the values obtained from the proposed method for all wavelengths to avoid the difficulty of reading ln F_0 from different files.

Along with the T values of three wavelengths obtained from Eq. (1), we use precipitable water content (PWC) and spectral surface albedo data, which are obtained from radiosonde observations (http://weather.uwyo.edu/upperair/sounding.html) and MODIS observations (product name: MCD43A4), respectively. Finally, COD and CER are retrieved simultaneously by minimizing the cost function (J).

$$J = (\boldsymbol{x} - \boldsymbol{x}_{\mathrm{a}})^T \boldsymbol{S}_{\mathrm{a}}^{-1} (\boldsymbol{x} - \boldsymbol{x}_{\mathrm{a}}) + [\boldsymbol{y} - \boldsymbol{F}(\boldsymbol{x}, \boldsymbol{b})]^T \boldsymbol{S}_{\mathrm{y}}^{-1} (\boldsymbol{y} - \boldsymbol{F}(\boldsymbol{x}, \boldsymbol{b})] \tag{2}$$

where $\boldsymbol{x}$ is a state vector, $\boldsymbol{x}_{\mathrm{a}}$ is an a priori vector, $\boldsymbol{S}_{\mathrm{a}}$ and $\boldsymbol{S}_{\mathrm{y}}$ are error covariance matrices for the a priori and measurement, respectively, $\boldsymbol{y}$ is the measurement vector, $\boldsymbol{F}$ is the forward model, and $\boldsymbol{b}$ is the model parameter vector (ancillary data). The terms $\boldsymbol{x}$, $\boldsymbol{y}$, and $\boldsymbol{b}$ are defined as

$$\boldsymbol{x} = \begin{pmatrix} \ln \tau \\ \ln r_{\mathrm{e}} \end{pmatrix}, \quad \boldsymbol{y} = \begin{pmatrix} \ln T_{1.627} \\ \ln T_{1.02} \\ \ln T_{0.87} \end{pmatrix}, \text{ and } \boldsymbol{b} = \begin{pmatrix} W \\ A_{1.627} \\ A_{1.02} \\ A_{0.87} \end{pmatrix},$$

where τ and r_e are COD and CER, respectively. W and A_λ are the PWC and surface albedo at wavelength λ, respectively. Both $\boldsymbol{S}_{\mathrm{a}}$ and $\boldsymbol{S}_{\mathrm{y}}$ are assumed to be diagonal matrices. $\boldsymbol{x}_{\mathrm{a}}$ and the diagonal elements of $\boldsymbol{S}_{\mathrm{a}}$ are determined from 1-year data for water cloud properties observed over Japanese SKYNET sites by the Advanced Himawari Imager (AHI) sensor onboard Himawari-8, a Japanese geostationary satellite. The diagonal terms for $\boldsymbol{S}_{\mathrm{y}}$ are determined based on simulation of perturbations in $T(\lambda)$ generated from 300 random gaussian noises of error sources, as discussed in Section 4. The Santa Barbara DISORT Atmospheric Radiative Transfer model (Ricchiazzi et al., 1998) is used for forward modeling, and the Levenberg–Marquardt method is used to minimize the cost function. The total number of iterations is set as 50. If the solution does not converge within 50 iterations, the analysis is discarded. As highlighted in Sections 1 and 4, transmittance signals may not always be characterized by unique COD or CER values. Consequently, the initial values of COD and CER used for iteration can be important when searching the plausible set of COD and CER values. To address this

Deleted: till …ntil the condition of the correlation coefficient ($r \geq 0.997$) is satisfied. To understand the quality of thus …he calculated ... [28]

Formatted ... [29]

Deleted: determined …rom an independent standard ... [30]

Formatted: Not Superscript/ Subscript

Deleted: is shown …or three different sky radiometers ... [31]

Formatted: Font: Not Bold

Deleted: °

Formatted: Font: Not Bold

Deleted: °

Formatted: Font: Not Bold

Deleted: °

Formatted: Font: Not Bold

Deleted: °

Formatted: Font: Not Bold

Deleted: °

Formatted: Font: Not Bold

Deleted: °…). Figure 2 shows a very…here is good ... [32]

Formatted ... [33]

Deleted: very…useful while …or analyzing data of …ong- ... [34]

Formatted ... [35]

Deleted: . They … which are obtained from radiosonde ... [36]

Deleted: … ... [37]

Formatted ... [38]

Deleted: … The terms $\boldsymbol{x}$, $\boldsymbol{y}$, and $\boldsymbol{b}$ are defined as: ... [39]

Formatted: Font: Not Italic

Deleted: represent …re COD and CER, respectively; ... [40]

Formatted: Font: Not Italic

Deleted: represent

Formatted ... [41]

Deleted: one…-year data of ... [42]

Formatted ... [43]

Deleted: section …ection 4. The Santa Barbara DISORT ... [44]

important issue, we first approximate the initial COD and CER values to start the iteration. The approximation is done by searching a set of COD and CER values by comparing observed $T_{1.02}/T_{1.627}$ and $T_{1.02}$ with LUT of corresponding values modeled for COD values of 1–64 and CER values of 2–32 µm in steps of 1 µm. $T_{1.02}/T_{1.627}$ decreases with the increase of COD; whereas when COD increases, $T_{1.02}$ increases first until reaching the peak value, and then starts to decrease. Thus, $T_{1.02}/T_{1.627}$ and $T_{1.02}$ can be used simultaneously to determine the range of COD and CER in which the true values are likely to fall. A set of COD and CER values that generate the smallest root mean square difference between the observed and modeled values is used for the initial values in the iteration.

4 Retrieval error

To understand the performance of the proposed algorithm for different types of input data (transmittance and ancillary data), retrieval errors are calculated by assuming errors on them. The retrieval errors are calculated for COD and CER values in the ranges of 1–64 and 2–32 µm, respectively, in steps of 1 µm. The simulations are performed for solar zenith and azimuth angles of 30° and 0°, respectively, by assuming that the cloud phase is water cloud. We assume 1% error in ln $F_0(\lambda)$, which is significantly larger than the maximum error in ln $F_0(\lambda)$ shown in Figure 2 and discussed in Section 3. This large error in ln $F_0(\lambda)$ is assumed to incorporate errors in $T(\lambda)$ generated from other possible factors, such as radiance measurement and $\Delta\Omega(\lambda)$ estimation. Similarly, we assume a surface albedo of 0.15 for all three wavelengths and PWC of 1.5 cm by assuming errors of ±0.025 and 1.0 cm, respectively. $F_0(\lambda)$ in actual data analysis is the instrument signal equivalent to the measurement performed at the top of the atmosphere (TOA); however, the incident irradiance at TOA (unit: W/m²/nm) calculated from the radiative transfer model for error evaluation simulations is discussed in this section. For each set of known COD and CER, 100 random gaussian noises for each error source are added in the retrieval to simulate 300 sets of COD and CER. The successful retrievals ($J \leq 3$) are used to calculate the mean bias error (MBE) as

$$MBE = \frac{\sum_{i=1}^{n}(\frac{S_i}{T_r} - 1)}{n} \quad (3),$$

where S_i and T_r are the simulated and true values, respectively. Only the MBE is discussed here because the error map evaluated in other forms, such as root mean square error (RMSE), contains the same qualitative information. Figure 3 shows the MBE for COD (first column), MBE for CER (second column), and total number of successful retrievals (third column) for each type of error separately and in combination. Figure 3(a)–3(c), 3(d)–3(f), 3(g)–3(i), and 3(j)–3(l) show the errors in transmittance, surface albedo, PWC, and all sources, respectively. The 100% unsuccessful retrieval is shown in black. The retrieval is more uncertain mainly when COD is less than ~15. Regardless of the error source, the retrieval error is high, especially for small (CER < ~7 µm) and large (CER > ~13 µm) cloud droplets. In general, the error domains of CER are expanded by overlapping the error domains of COD. This suggests that the error in input data affects CER retrieval more than COD retrieval. Among the three error sources, the error in transmittance can dominate the effect of the remaining two error sources. The successful retrieval number corresponding to each error source suggests that in the domains ~8 < COD < ~16 with CER > ~13 µm and CER < ~7 µm, the algorithm has difficulty fitting the measured transmittances with modeled values. These domains have high retrieval errors (first and second columns). The high errors

Deleted: values of …OD and CER values to start the iteration. It …he approximation is done by searching a set of COD and CER values through a …y comparison of…ng observed $T_{1.02}/T_{1.627}$ and $T_{1.02}$ with LUT of corresponding values modeled for COD values ranging from …f 1 … …4 and CER ranging …alues offrom…2 … …2 µm at …n steps of 1 µm. $T_{1.02}/T_{1.627}$ decreases with the increase of COD; whereas when COD increases, $T_{1.02}$ increases first until reaching the peak value, and then starts to decrease. Thus, simultaneous use of …$_{1.02}/T_{1.627}$ and $T_{1.02}$ can be used simultaneously can help one …o figure out…etermine the range of COD and CER,…in which the true values are likely to fall. A set of COD and CER values that can…generate a least…he smallest root mean square difference between the observed and modeled values is used as ... [45]

Deleted: In order t

Formatted: Indent: First line: 0 ch

Deleted: intervals …anges of 1 - …64 and 2 - …32 µm, respectively, with …n steps of 1 µm. The simulations are ... [46]

Formatted ... [47]

Deleted: . …re 2 and discussed in section ... [48]

Deleted: also

Formatted ... [49]

Formatted ... [50]

Deleted: on them…f as…±0.025 and 1.0 cm, respectively. Though ... [51]

Formatted ... [52]

Deleted:), …; however, it is …he incident irradiance at TOA (unit: W/m²/nm) calculated from the radiative transfer ... [53]

Deleted:

Deleted: ,

Deleted: represent …re the simulated and true values, respectively. Only the MBE is discussed here because the ... [55]

Formatted ... [54]

in COD and CER are extended further for COD < ~8 despite the sufficient number of successful retrievals. The contour lines for $T(\lambda)$ in Figure 4(a), 4(b), and 4(c) for wavelengths of 0.87, 1.02, and 1.627 µm, respectively, can help to understand these domains. The $T(\lambda)$ values in Figure 4(a)–4(c) correspond to no error in the input data.

For unsuccessful retrievals for the ~8 < COD < ~16 and CER > ~13 µm domain, the $T(\lambda)$ values hardly change as CER increases above ~13 µm (Figure 4(a)–4(c)). As a result, the CER retrieval above ~13 µm is uncertain and the retrieved CER is generally underestimated. $T(\lambda)$ contour lines falling within ~8 < COD < ~16 appear again for COD < ~2. Therefore, to search for the best set of COD and CER by trying to fit the inputted $T(\lambda)$ values with the modeled values, the algorithm can mistakenly search for a plausible solution in this small COD domain. If this happens, the retrieval may not be confined within $J \leq 3$. The algorithm is likely to compensate for such underestimated CERs by overestimating CODs (Figure 3(a) and 3(b), and 3(j) and 3(k)).

Similarly, for failed retrievals for CER < ~7 µm, a non-uniform change in T(1.627 µm) associated with the change in CER (Figure 4(c)), can be an important factor. The non-uniform response of CER to the change T(1.627 µm) can mislead the algorithm while searching for the best set of COD and CER and may force the algorithm to shift wrongly to the COD < ~2 domain to search for a plausible solution. Both CER and COD may be overestimated for CER > ~7 µm.

Despite a sufficient number of successful retrievals, there are high errors in the retrieved values for COD < ~8. Similar to the error domains, the retrieval errors are mainly confined to large and small values of CER. The peak values of $T(\lambda)$ generally decrease for ~3 ≤ COD ≤ ~6. Because both the forward scattering and absorption increase with the increase of COD and the increase in multiple scattering, the increase in $T(\lambda)$ before the peak value is due to the dominance of forward scattering over absorption, and vice versa for the decrease in $T(\lambda)$ after the peak value. In other words, the competition between forward scattering and absorption is maximum to increase or decrease $T(\lambda)$ within this COD range [[Please clarify your meaning here.]]. CER is as important as COD in the increase or decrease of $T(\lambda)$, and the algorithm must consider changes in COD and CER while searching for a plausible set of COD and CER. Thus, it [[Please clarify what "it" refers to here. Do you mean "The domain ~3 ≤ COD ≤ ~6"?]] is the most sensitive COD range for the ambiguous solution of COD and CER in transmittance-based remote sensing. Therefore, even a small degree of error in input data can change both COD and CER considerably from their true values. Though weak, this change may still occur in this COD range, causing errors in retrieved values even for COD < ~3. The weak CER response towards $T(\lambda)$ for large CERs plays an important role in introducing errors in retrieved values for large CERs. A complicated distribution of T(1.627 µm) for CER < ~7 µm may be an important factor for errors in small CERs, and the appearance of the same $T(\lambda)$ values for larger CODs may be the next important factor for errors in COD < ~2.

Overall, the retrieval error in COD is smaller than that in CER for domain coverage and error magnitude, suggesting that the transmittance-based cloud remote sensing is better for COD retrieval than for CER retrieval. Except for a limited number of error domains, the magnitudes of the retrieval errors are small. For example, for COD > 15 and all types of errors, the 5th, 50th, and 95th percentile values of MBE for retrieved COD are -2.0%, -0.6%, and 0.82%, respectively, and for retrieved CER they are -4.1%, -0.51%, and 7.2%, respectively. For reference, the maximum (minimum) retrieval errors for COD ≥ 20 and CER = 10 µm for a spectral method proposed by McBride et al. (2011) are ~7% (~2%) and

Deleted: further …xtended further for COD < ~8 despite ... [56]

Deleted: shown…in Figs.…re 4(a), 4(b), and 4(c) for the ... [58]

Formatted ... [57]

Formatted ... [59]

Deleted: shown …n Figs.…re 4(a) … …(c) correspond to ... [60]

Deleted: First talking about…or unsuccessful retrievals ... [61]

Deleted: can …ardly change with the…s increase of …ER ... [63]

Formatted ... [62]

Formatted ... [64]

Deleted: get …ppear again for COD < ~2. Therefore, in an ... [65]

Formatted ... [66]

Deleted: the …or a plausible solution from …n this small ... [67]

Deleted: talking about…or failed retrievals for CER < ~7 ... [68]

Formatted: Font: Not Italic

Deleted: change, as shown by… …ig. …re 4(c)), can be the ... [69]

Formatted: Font: Not Italic

Deleted: change …an mislead the algorithm while searching ... [70]

Formatted ... [71]

Deleted: fall

Formatted: Not Highlight

Deleted: As …ecause both the forward scattering and ... [72]

Formatted ... [73]

Deleted: opposite

Formatted ... [74]

Deleted: Not only COD, but also …ER is equally …s ... [75]

Formatted ... [76]

Deleted: needs to take into account of…ust consider both ... [77]

Formatted ... [78]

Deleted: …ased remote sensing. Therefore, even a small ... [79]

Formatted ... [80]

Deleted: , as discussed above,…again …lays an important ... [81]

Formatted: Font: Not Italic

Deleted: , as discussed above, can…ay be an important ... [82]

Formatted ... [83]

Deleted: , as discussed above, can…ay be the next important ... [84]

Deleted: speaking… the retrieval error in COD is smaller ... [85]

~52% (~14%) for COD and CER, respectively. In Section 5, we examine the quality of the retrieved cloud properties based on comparison with standard data obtained from independent sources.

5 Comparison with data from independent sources

5.1 Solar radiation data

The broad-band radiance and irradiance of the shortwave spectral range (0.3–2.8 μm) were observed using a narrow-angle radiometer ([[Please include the model name.]], Kipp and Zonen, Netherlands; FOV: 5°) and a pyranometer ([[Please include the model name.]], EKO Instruments Co., Ltd., Japan; FOV: 180°), respectively, at Chiba (35.62°N, 140.10°E) every 20 s from December 2015 to December 2016 to evaluate the cloud properties observed by the sky radiometer. The narrow-angle radiometer [[Please confirm.]] observes the downwelling irradiance signals as voltage in a narrow FOV. The instrument was calibrated by the manufacturer in the laboratory, and the observed signals are converted into radiance (unit: W/m^2/sr) by using the constant calibration value. Because the sensor faces upward and the instrument's FOV is narrow, the instrument measures the downwelling radiance of the zenith direction. The cloud properties from the sky radiometer are combined with the surface albedo observed by MODIS and the PWC observed by radiosonde to calculate the corresponding observations. A comparison is performed for an average of 5 min observation of solar radiation that centers the sky radiometer observation time. Figures 5(a) and 5(b) compare the broad-band radiance and irradiance, respectively. For reference, a comparison is also performed for modeled values using cloud properties from AHI instead of the sky radiometer for broad-band radiance and irradiance (Figures 5(c) and 5(d)).

For cloud properties from the sky radiometer, there is a strong (weak) correlation between modeled and observed values for broad-band radiance (irradiance). In contrast, for AHI cloud properties, the correlation between the modeled and observed values for broad-band radiance (irradiance) is weak (strong). Compared with data from the pyranometer [[Please confirm or clarify your meaning here.]], the observed data from the narrow-angle radiometer best describes the quality of the sky radiometer cloud properties because of the narrow FOV. The good agreement in Figure 5(a) with a correlation coefficient (r) of up to 0.93 suggests that sky radiometer cloud properties (at least COD) are qualitative enough. Because the contribution of COD is greater than that of CER to broad-band solar radiation (Khatri et al., 2018), Figure 5(a) alone cannot explain the quality of the retrieved CER. The poor agreement for irradiance comparison in Figure 5(b) can be explained by the large difference in FOV of the sky radiometer and pyranometer; the surface observed solar radiation varies drastically depending on the instrument FOV. For example, in the scatter plot for broad-band irradiance observed by pyranometer and radiance observed by a narrow-angle radiometer at Chiba during January–March 2016, the correlation is poor (Figure 6). An important factor in decreasing the correlation between these measurements is the cloud horizontal inhomogeneity, which can explain the poor agreement in Figure 5(b) plausibly, despite the accurate retrieval from the sky radiometer (Figure 5(a)). In contrast, the AHI cloud properties are average or representative values of specific coverage, for instance, a pixel (e.g., 1 × 1 km). As a result, the irradiances modeled with the AHI cloud properties are closer to the observed irradiance than those modeled with the sky radiometer cloud properties. This is because the cloud observed by the sky radiometer can be a small portion of a pixel containing horizontally inhomogeneous clouds.

Deleted: Below, …n section …ection 5, further sheds light on ... [86]

Deleted: … ... [87]

Formatted: Highlight

Moved (insertion) [1]

Formatted: Font: Not Bold

Deleted: °

Deleted: °…) at each…very 20 seconds…from December 2015 to December 2016 using a narrow-angle (NA) radiometer (FOV: 5°) and a pyranometer (FOV: 180°), respectively are used for the…o evaluation …valuate theof…sky radiometer observed …loud properties observed by the sky radiometer. The broad-band irradiance and broad-band radiance of spectral range mentioned above are observed by instruments manufactured by Kipp and Zonen, Netherland and EKO Instruments Co., Ltd., Japan, respectively. ... [88]

Formatted: Font: Not Bold

Moved up [1]: EKO Instruments Co., Ltd., Japan

Deleted: latter

Formatted ... [89]

Deleted: can …bserves the downwelling irradiance signals in terms of…s voltage at …n a very…narrow FOV. The instrument was calibrated by a …he manufacturer in the laboratory, and by using such calibration constant value,…it is possible to convert …he observed signals are converted into radiance of …unit: W/m^2/sr) by using the constant calibration value. As …ecause the sensor faces upward and the instrument's FOV is narrow, the signal measured by ... [90]

Deleted: Firstly, one can see…here is a strong (weak) correlation between modeled and observed values for broad- ... [91]

Formatted ... [92]

Deleted: NA…radiometer observed data can …est describes the quality of the sky radiometer cloud properties because of ... [93]

5.2 Satellite cloud products

As part of validating the water cloud products of MODIS and AHI using surface radiation data, Khatri et al. (2018) compared water cloud properties retrieved from sky radiometers at the SKYNET observation sites of Chiba, Hedo-misaki, and Fukue-jima with those of MODIS and AHI observations for October 2016 to December 2017. They used surface irradiance data, and the validation results using sky radiometer and surface irradiance data were qualitatively similar. A good (poor) agreement was shown for COD (CER) between sky radiometer and satellite products in Khatri et al. (2018). They compared sky radiometer results with results of collocated satellite pixels by selecting samples with a time difference of less than 1.25 min, which is half the temporal resolution of the AHI observations over Japan. The distance between the pixel center and the observation site was less than 1 km, and they performed parallax correction for satellite products.

In Section 5.1, we identified the inhomogeneous clouds and broken clouds in the satellite pixels as major obstacles in assessing the quality of satellite products using the sky radiometer results and vice versa. Here, we examine the quality of sky radiometer products by using satellite products. We prepare samples for comparison by addressing the cloud inhomogeneity problem in a logical way with the available information. If the surface irradiance calculated from the sky radiometer cloud properties agrees well with that observed at the surface, the effective COD of the actual inhomogeneous clouds may be represented by a sky radiometer COD. The effective COD refers to the COD of the assumed plane-parallel homogenous cloud layers, which can produce irradiance equivalent to that produced by actual inhomogeneous clouds, that is, the measured irradiance. The satellite cloud properties retrieved from reflected signals assume clouds are plane-parallel homogenous layers. The sky radiometer cloud properties that generate surface irradiances equivalent to observed values by differing by not more than 1% are compared with the satellite cloud properties. Figure 7(a) and 7(b) compare the sky radiometer CODs with MODIS and AHI values, respectively, for the same sites and period as Khatri et al. (2018). The COD agreement is good. The results are qualitatively same for both MODIS and AHI, with *r* values of ~0.6 and ~0.7 and RMSE values of ~13 and ~10 for MODIS and AHI, respectively. Despite several differences between the sky radiometer and satellite products from observation and retrieval, their good agreement indicates that they have a similar response towards thin and thick clouds, although the COD values may not be identical. Similarly, Figures 8(a) and 8(b) compare the sky radiometer CERs with MODIS and AHI values, respectively. The water absorbing wavelengths corresponding to MODIS and AHI are 2.1 and 3.79 µm, respectively. The CERs between the sky radiometer and satellite sensors are poorly correlated, with *r* less than 0.12 and RMSE of ~7 µm for both satellite sensors. This poor correlation may be mainly due to the high sensitivity toward cloud top layers of the satellite sensors using reflected signals (Platnick, 2000), whereas sky radiometers are sensitive to all the cloud layers.

Although the qualitive information reported by Khatri et al. (2018) and the comparisons in Figures 7 and 8 of this study are similar, there are differences in Figures 7 and 8 with the comparison plots shown in Khatri et al. (2018). The application of data screening criteria generally screened out data with large differences between the sky radiometer and satellite sensors. These large differences in the previous comparison probably arose from the different FOVs of the

Deleted: for three observation sites of SKYNET: Chiba, Hedo-misaki, and Fukue-jima …or the period of October,…2016 to December,…2017. They further …sed surface irradiance data, and found that …he validation results using sky radiometer and surface irradiance data are were qualitatively similar same… A fairly …ood (poor) agreement was shown for COD (CER) between sky radiometer and satellite products in Khatri et al. (2018). They compared sky radiometer results with results of collocated satellite pixels by selecting samples with a time difference of less than 1.25 minutes… which is half of …he temporal resolution of the AHI observations over Japan, … and t…he distance between the pixel center and the observation site was less than 1 km, and further doing ... [94]

Deleted: It is learnt from…n section …ection 5.1, we identified that…the inhomogeneous clouds and/or…broken clouds contained within…n the satellite pixels are …s major obstacles in quality …ssessment…ng the quality of satellite products using the sky radiometer results and vice versa. This section…ere, we attempts to improve our understating regarding…examine the quality of sky radiometer products ... [95]

Deleted: at hand… If the surface irradiance calculated from the sky radiometer cloud properties agrees well with that observed at the surface, the effective COD of the actual inhomogeneous clouds may be represented by a sky radiometer COD. Here, …he effective COD refers to the COD of the assumed plane-parallel homogenous cloud ... [96]

Formatted: Not Highlight

Deleted: Though …lthough the qualitive information revealed from…eported by Khatri et al. (2018) and the comparisons results of…in Figures 7 and 8 of this study are in general the same…imilar, there are some …ifferences in Figures 7 and 8 with respect to…he comparison plots shown in Khatri et al. (2018). Application …he application of data ... [97]

satellite sensor and sky radiometer, while observing inhomogeneous clouds. Thus, the comparison results presented in this study by addressing the cloud inhomogeneity problem more logically should give more accurate and refined information than those presented in Khatri et al. (2018).

6 Conclusions

To make cloud observation from the surface more common and convenient, we developed an algorithm to retrieve cloud properties (COD and CER) from spectral zenith radiances measured by sky radiometer. By considering a priori information of the state vector and errors related to observed transmittance and using ancillary data (PWC and surface albedo), an optimal estimation approach was proposed by fitting the observed transmittances at wavelengths of 0.87, 1.02, and 1.627 µm with modeled values. To ease data analysis of long-term observations further by overcoming the filter degradation problem, an on-site method of calibrating for direct intensity was proposed by using aerosol data for clear sky days. The calibration constants derived from the proposed method agree well with values determined by collocating the field instruments with the master instrument. The retrieval error analyses performed by considering known ranges of errors in the observed transmittances and ancillary data suggested that the algorithm performed well, except for in narrow bands of small COD and CER values. In general, the errors in input information affected CER retrieval more strongly than COD retrieval, and the retrieved CER had large errors when clouds are optically thin (COD < ~15) and cloud droplets are small (CER < ~7 µm) or large (CER > ~13 µm). As part of the quality assessment, cloud properties retrieved from the proposed algorithm were compared indirectly with surface observed radiance and irradiance data and directly with observed cloud properties from MODIS and AHI. The retrieved cloud properties produced broadband shortwave radiances similar to those observed by a narrow-angle radiometer, confirming the good quality of the retrieved products (at least COD) from the sky radiometer. However, the agreement was poor when broadband shortwave irradiances observed by a pyranometer with a wide FOV were compared with the modeled values. This discrepancy was probably caused by the large difference in FOVs between the sky radiometer and pyranometer, suggesting that the instrument's FOV has a large effect on cloud remote sensing. COD agreed well between the sky radiometer and satellite sensors; however, the agreement was poor for CER.

Figure 1: Schematic of the study method.

Figure 2: Comparison of the direct intensity calibration constant (ln F_0) values at the water absorbing wavelength of 1.627 µm for the standard method (calibration using the master instrument) and our on-site method for sky radiometers at Hedo-misaki (26.87°N, 128.25°E), Fukue-jima (32.75°N, 128.68°E), and Sendai (38.26°N, 140.84°E). The difference (%) is also shown, which is the difference (percentage) between the proposed method and the standard method normalized by the value of the standard method.

Deleted: such …loud inhomogeneity related …roblem more logically is expected to ... [98]

Deleted: In an effort of making…o make cloud observation from the surface more common and convenient, this study…e develops …eveloped an algorithm to retrieve cloud properties (COD and CER) from spectral zenith radiances measured by sky radiometer. By taking into account of considering a priori information of …f the a …tate vector and errors related to observation based…d transmittance and used …sing ancillary data (PWC and surface albedo), an optimal-…estimation approach is …as proposed by fitting the observation based…d transmittances at the …avelengths of 0.87, 1.02, and 1.627 µm with modeled values. To further ease data analysis of long-term observations further by overcoming the filter degradation problem, an on-site method of calibration …alibrating for direct intensity is …as proposed by making use of…sing aerosol data of very…or clear sky days. The calibration constants derived from the proposed method agree quite …ell with values determined by collocating the field instruments with the master instrument. The retrieval error analyses performed by considering known ranges of errors in the observation based…d transmittances and ancillary data suggested a good performance of…hat the algorithm performed well, except for a certain…n narrow bands of small COD and CER values. In general, the errors in input information can ... [99]

Deleted: A s…chematic diagram ... [100]

Formatted: Font: Italic

Deleted: between …or the standard method (calibration using the master instrument) and an …ur on-site method proposed in this study …or sky radiometers belonging to…t Hedo-misaki (26.87°°…, 128.25°°…), Fukue-jima (32.75°°…, 128.68°°…), and Sendai (38.26°°…, 140.84°°…). Shown in the figure is also t…he difference ... [101]

Figure 3: Mean bias error (MBE) values for retrieved (a) cloud optical depth (COD) and (b) cloud particle effective radius (CER), and (c) total number of successful retrievals for assumed error in transmittance; (d)–(f): same as upper panel but for assumed error in surface albedo; (g)–(i): same as upper panel but for assumed error in precipitable water content; (j)–(l): same as upper panel but for all error sources. The 100% unsuccessful retrieval is shown in black.

Figure 4: Contour plots of transmittances at wavelengths of (a) 0.87, (b) 1.02, and (c) 1.627 µm for solar zenith and azimuth angles of 30° and 0°, respectively. The transmittance values are given within the contour lines. Different colors are used for 1.627 µm to make it easy to distinguish. COD, cloud optical depth; CER, cloud particle effective radius.

Figure 5: Comparison of modeled and observed broad-band (a) radiances and (b) irradiances for modeled values using sky radiometer cloud proprieties for the observation site at Chiba (35.62°N, 140.10°E) for 2016. (c) and (d) Comparison results for broad-band radiances (c) and (d) irradiance for modeled cloud properties corresponding to the Advanced Himawari Imager.

Figure 6: Scatterplot of broad-band radiances and irradiances observed with a narrow-angle radiometer and a wide-angle pyranometer at Chiba (35.62°N, 140.10°E) during January–March 2016. The solid line represents $y = 2\pi x$.

Figure 7: Comparison of sky radiometer cloud optical depths (CODs) with (a) MODIS and (b) Advanced Himawari Imager CODs for observation sites at Chiba (35.62°N, 140.10°E), Hedo-misaki (26.87°N, 128.25°E), and Fukue-jima (32.75°N, 128.68°E) from October 2015 to December 2016.

Figure 8: Same as Figure 7, but for comparison of sky radiometer cloud particle effective radiuses (CERs).

Formatted: Font: Bold

Deleted: in (a), (b) and (c), respectively…for assumed error in transmittance; (d) … …f): same as upper panel but for assumed error in surface albedo; (g) … …i): same as upper panel but for assumed error in precipitable water content; (j) … …l): same as upper panel but for all error sources. The 100% unsuccessful retrieval is denoted by…hown in black color… ... [102]

Deleted: the …avelengths of (a) 0.87 µm… (b) 1.02 µm… and (c) 1.627 µm for solar zenith and azimuth angles of 30° and 0°, respectively. The values of transmittances…values are given within the contour lines. Different colors are used for 1.627 µm to make it easy to distinguish. ... [103]

Deleted: between …f modeled and observed broad-band (a) radiances and (b) irradiances for modeled values using sky radiometer cloud proprieties for the observation site of …t Chiba (35.62°°…, 140.10°°…) for 2016. Similarly, …c) and (d) show the c…omparison results for broad-band radiances (c) and (d) irradiance, respectively…for modeled cloud properties corresponding to the Advanced Himawari ImagerAHI ... [104]

Deleted: by radiometers of …ith a narrow-angle radiometer and a wide-angle (…yranometer), respectively…at Chiba (35.62°°…, 140.10°°…) during ... [105]

Deleted: AHI…CODs for observation sites of …t Chiba (35.62°°…, 140.10°°…), Hedo-misaki (26.87°°…, 128.25°°…), and Fukue-jima (32.75°°…, 128.68°°…) for from periods of …ctober,…2015 to December, ... [106]

Deleted: comparison… ... [107]